Bioorganic Chemistry 157 (2025) 108316

Contents lists available at ScienceDirect

Bioorganic Chemistry

journal homepage: www.elsevier.com/locate/bioorg

Identification of a novel Azaspirooxindolinone-based PROTAC for selective BTK degradation and enhanced anticancer activity

Naveen Kumar Rampeesa [a,b], Rambabu Gundla [a,*], Gopal Mudasani [a,b], Sudhakar Tangallapalli [a], Sreenivasa Reddy Anugu [b], Soňa Gurská [c,d], Juan Bautista De Sanctis [c,d], Petr Džubák [c,d], Marián Hajdúch [c,d], Viswanath Das [c,d,**]

[a] Department of Chemistry, School of Science, GITAM University, Hyderabad 502102, Telangana, India
[b] Aragen Life Sciences Ltd, Medicinal Chemistry Laboratory Division, Survey, No: 125(Part) & 126, IDA Mallapur, Hyderabad 500076, India
[c] Institute of Molecular and Translational Medicine, Faculty of Medicine and Dentistry, Palacký University and University Hospital Olomouc, Hněvotínská 1333/5, 779 00 Olomouc, Czech Republic
[d] Institute of Molecular and Translational Medicine, Czech Advanced Technologies and Research Institute, Palacký University Olomouc, Křížkovského 511/8, 779 00, Olomouc, Czech Republic

ARTICLE INFO

Keywords:
Antiproliferative activity
Azaspirooxindolinone
Bruton's tyrosine kinase
Jurkat
IL-2-inducible T-cell kinase
PROTAC
Ramos

ABSTRACT

Bruton's Tyrosine Kinase (BTK) is a key driver of hematological malignancies, autoimmune disorders, and neuroinflammation, making it an attractive therapeutic target. Proteolysis targeting chimeras (PROTACs) offer a novel strategy for BTK degradation via the E3 ubiquitin ligase pathway. Here, we evaluated nine azaspirooxindolinone-based PROTAC derivatives for their cytotoxicity and BTK-targeting activity. Several compounds exhibited potent cytotoxicity against BTK-high RAMOS lymphoma cells without affecting non-cancer fibroblasts or normal T/B-cell lymphocytes. Among them, PROTAC **25** emerged as the most effective degraded, achieving a Dmax of 72.84 % and DC50 of 0.27 μM in a proteasome-dependent manner. Although PROTAC **25** was cytotoxic to IL-2-inducible T cell Kinase (ITK)-positive cells, ITK protein levels remained unaffected. Furthermore, kinase assays revealed that PROTAC 25 inhibited BTK kinase activity (IC_{50} = 0.44 μM) with moderate selectivity over ITK (IC_{50} = 2.16 μM). Notably, PROTAC **25** suppressed BTK-mediated downstream signaling in RAMOS cells, as evidenced by reduced phosphorylation of BTK and its downstream effector, p38 MAPK. These findings highlight PROTAC **25** as a promising BTK degrader with therapeutic potential and underscore the value of azaspirooxindolinone-based PROTACs in targeting BTK-driven diseases.

1. Introduction

Bruton's Tyrosine Kinase (BTK), a non-receptor protein-tyrosine kinase of the Tec family, plays a critical role in hematopoietic cell signaling [1]. Aberrant BTK activity is implicated in various human diseases, including B-cell malignancies, autoimmune diseases, and neuroinflammation [2–4]. Beyond its role in B cells, BTK contributes to mast cell, macrophage, and dendritic cell functions, underscoring its potential as a therapeutic target [5]. Clinical studies have shown that targeting BTK can enhance treatments for diseases such as chronic lymphocytic leukemia and multiple sclerosis by modulating immune cell functions [6,7]. However, resistance mutations, such as C481S, reduce the efficacy of covalent BTK inhibitors like ibrutinib, creating an urgent need for alternative therapeutic strategies [8–10].

Proteolysis targeting chimeras (PROTACs) have emerged as a transformative approach for selective protein degradation, overcoming the limitations of traditional inhibitors. Recent advancements have highlighted the potential of BTK-targeting PROTACs to overcome resistance mutations, including the C481S while offering sustained suppression of BTK-mediated signaling pathways [8,11–13]. For example, NX-2127, a BTK PROTAC in clinical trials, not only degrades BTK but also modulates immune responses via CRBN-mediated degradation of neosubstrates IKZF1/3 [14].

This study focuses on developing azaspirooxindolinone-based

* Corresponding author.
** Corresponding author at: Institute of Molecular and Translational Medicine, Faculty of Medicine and Dentistry, Palacký University and University Hospital Olomouc, Hněvotínská 1333/5, 779 00 Olomouc, Czech Republic.
E-mail addresses: rgundla@gitam.edu (R. Gundla), viswanath.das@upol.cz (V. Das).

https://doi.org/10.1016/j.bioorg.2025.108316
Received 27 November 2024; Received in revised form 4 February 2025; Accepted 23 February 2025
Available online 26 February 2025

PROTAC derivatives designed to target BTK. While cell lines expressing IL-2 inducible T cell Kinase (ITK), another Tec family kinase [15], was included in cytotoxicity assays to explore potential off-target effects, the primary objective was to evaluate BTK degradation and its downstream impact. Building on our prior work with azaspirooxindolinone derivatives exhibiting activity against BTK and ITK-positive cell lines [16], we synthesized nine PROTAC derivatives to evaluate their anti-cancer potential. To enhance BTK selectivity and potency, we conducted structure-activity relationship (SAR) studies, focusing on PROTACs with varying linker lengths and compositions, motivated by the reported effectiveness of CRBN-based degraders such as PTD10 [9]. These linkers were carefully selected to optimize flexibility and spatial compatibility, facilitating efficient ternary complex formation, a critical step for enabling selective degradation via the proteasome pathway. We identified a hit compound, PROTAC **25**, which emerged as a selective BTK degrader with potent cytotoxicity in BTK-positive lymphoma cells and minimal off-target effects.

2. Result and discussions

2.1. Chemistry

The PROTACs were designed based on the azaspirooxindolinone derivative PT-II-12, previously synthesized by our group, which showed good cytotoxicity against ITK and BTK-positive cancer cell lines [16] (Fig. 1a). To enhance the activity of PT-II-12, the PROTAC strategy was employed by linking the azaspirooxindolinone scaffold, which targets BTK as the protein of interest (POI), to a CRBN-binding thalidomide moiety (Fig. 1b). Docking studies conducted prior to synthesis revealed that the piperidine ring of PT-II-12 and phenyl ring of thalidomide extended into a solvent-exposed region suitable for linker attachment, enabling POI binding and CRBN recruitment (Fig. 1c).

The linkers were selected based on reported data for CRBN-recruiting PROTACs, which emphasize the importance of linker length and composition in facilitating the ternary complex formation and effective protein degradation [17,18]. Specifically, PEG-based, alkyl chain and mixed linkers were chosen to ensure flexibility and spatial compatibility between the POI and CRBN. Using this strategy, we designed a library of PROTAC derivatives with varying linker lengths and compositions. From this library, nine compounds were selected for synthesis and evaluation based on interaction profiles and docking scores, prioritizing those predicted to form favorable interactions with BTK (Fig. 1d). These compounds were subsequently tested for their effect on BTK degradation and cellular activity.

To synthesize compound **3** (Scheme 1), azaspirooxindolinone **1** was treated with 5-fluoro thalidomide (**2**). For compound **7**, tertiary butyl glycine was first substituted with **2**, followed by tert-butyl deprotection (Scheme 1) and coupling with **1** (Scheme 2). Compound **10** was prepared by reacting to 7-amino heptanoic acid with **2** (Scheme 1), followed by amide coupling with **1** (Scheme 2). For compound **14**,

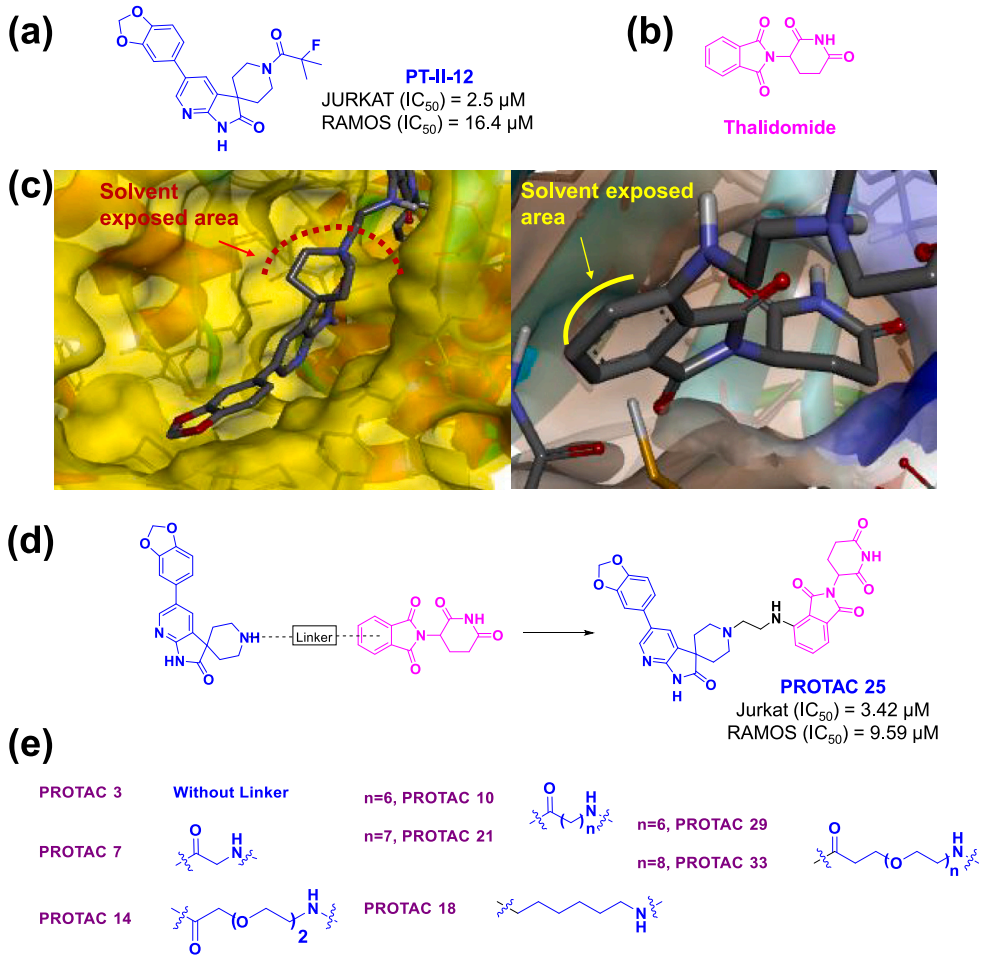

Fig. 1. Rational design of azaspirooxindolinone-based BTK-targeting PROTACs. (a) The parent azaspirooxindolinone compound, previously reported to exhibit cytotoxic activity against BTK-high RAMOS and ITK-positive Jurkat cells (IC_{50} = 2.5 μM and 16.4 μM, respectively) [16], was selected as the scaffold for targeting the POI. (**b**) Thalidomide was used as the E3 ligase recruiter to bind CRBN. (**c**) Docking studies identified solvent-exposed regions within the BTK binding pocket interacting with the azaspirooxindolinone scaffold (left) and thalidomide (right). (**d**) Design of PROTAC **25**, showing the azaspirooxindolinone scaffold (PT-II-12) linked to thalidomide via a 2-methylene chain linker. (**e**) Structures of alternative linkers used for generating different PROTAC derivatives.

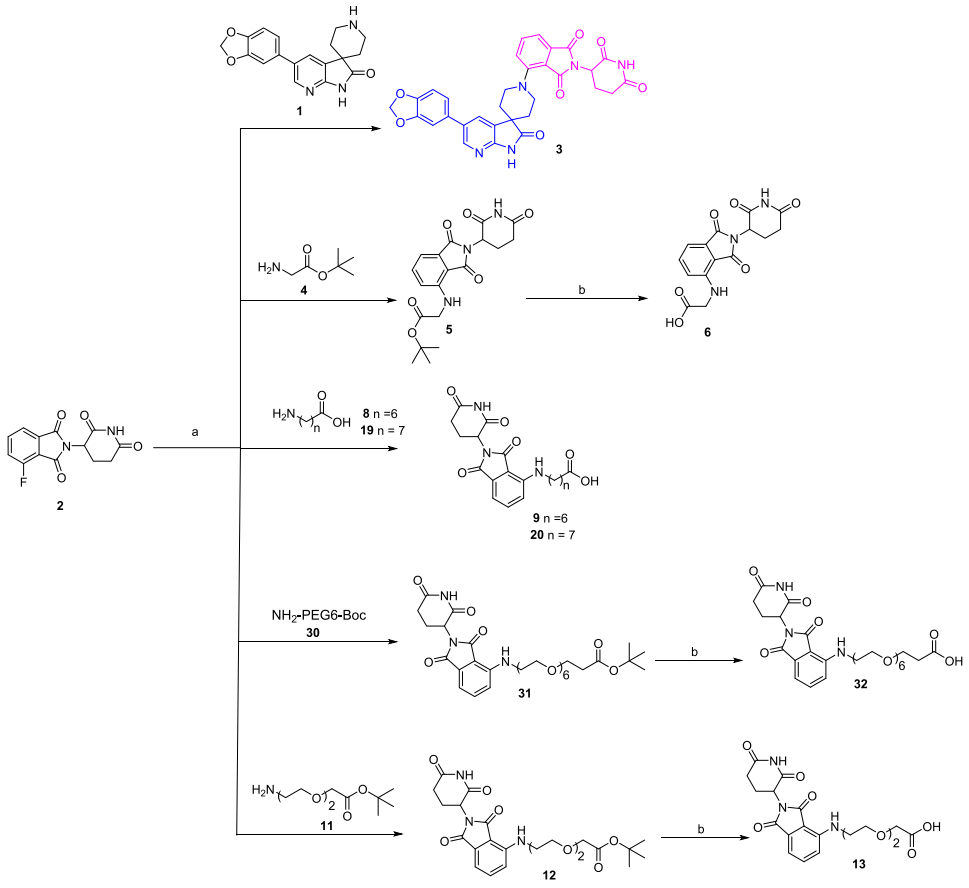

Scheme 1. Reaction conditions: a) DIPEA, DMSO, 100 °C, 1 h. b) TFA, DCM, RT, 16 h.

nucleophilic substitution of **11** with **2** was followed by deprotection (Scheme 1) and coupling with **1** (Scheme 2). Compound **18** was synthesized by treating **1** with **15**, followed by boc deprotection (Scheme 3) and substitution with **2** (Scheme 4). To obtain compound **21**, 8-amino octanoic acid was reacted with **2** (Scheme 1), followed by amide coupling with **1** (Scheme 2). For compound **25**, **1** was reacted with **22**, followed by boc deprotection (Scheme 3) and substitution with **2** (Scheme 4). Similarly, compound **29** was synthesized by reacting **1** with **26**, followed by boc deprotection (Scheme 2) and substitution with **2** (Scheme 4). Finally, for compound **33**, **2** was substituted with **30**, followed by tert-butyl deprotection (Scheme 1) and coupling with **1** (Scheme 2).

2.2. Docking analysis of PROTAC derivatives of azaspirooxindolinone

Building on prior docking studies, which guided the rational design of linkers by identifying solvent-exposed regions suitable for attachment, we evaluated the nine synthesized PROTAC derivatives for their interactions with the BTK active site. Ibrutinib bound to BTK (PDB ID: 5P9J) was used as a reference for comparison in these docking analyses. Table 1 shows a summary of the docking scores and the specific amino acid interactions for each of the tested compounds. PROTAC **3**, **7**, **10**, **14**, **18**, **21**, and **25** showed favorable interactions with key BTK resides, such as Thr474, Leu408, and Arg525, through various types of bonds. These findings are consistent with other studies demonstrating that BTK forms significant hydrogen bonds with residues, including Thr474, Met477, Leu408, and Arg525 [19,20]. Notably, PROTAC **25** displayed unique hydrogen bonds with Asp521 and Asn526, which were not observed together in the other PROTACs tested in this study (Fig. 2). Similar interactions have also been observed with the BTK inhibitor remibrutinib, which forms non-covalent bonds with residues such as Gln412, Phe413, Asp521, Asn526, and Tyr551 [21]. Due to these interactions with BTK, we next subjected the synthesized compounds to cytotoxicity profiling in a panel of ITK/BTK-null and ITK-BTK-positive cancer and non-cancer cell lines.

2.3. Evaluation of PROTAC cytotoxicity in ITK/BTK-positive and -null cell line panel

The cytotoxic efficacy of all nine PROTACs was evaluated in vitro in a panel of human cancer and non-cancer cell lines, positive or negative for ITK and BTK expression, and representing both sexes [22]. In total, 67 % of the cell lines were male-derived, and 33 % were female-derived. Among ITK- and BTK-positive cell lines, the distribution was evenly split between male and female (50 % each), while ITK/BTK-null lines comprised 80 % male and 20 % female (Table 2). Among ITK-positive cell lines, the female-derived CCRF-CEM consistently showed higher sensitivity than the male-derived JURKAT, with PROTAC **7** and **14** exhibiting lower IC_{50} values in CCRF-CEM. This increased sensitivity of parental CCRF-CEM may be due to inherent cellular mechanisms that make them more susceptible to cytotoxic agents [23]. For BTK-positive cell lines, the male-derived RAMOS displayed significant sensitivity to multiple compounds, whereas the female-derived K562 was resistant, likely due to the presence of the BCR-ABL fusion gene [24]. In ITK/BTK-null cell lines, no clear sex-specific differences were observed. Overall, the cytotoxic response was primarily influenced by ITK/BTK expression. However, subtle sex-specific differences were noted, particularly among ITK- and BTK-positive lines, indicating that biological differences related to sex may contribute to variations in sensitivity to our synthesized compounds. Further investigation is needed to confirm these findings, which is beyond the scope of this study.

Combining glycine as a linker with thalidomide (**2**) and our POI

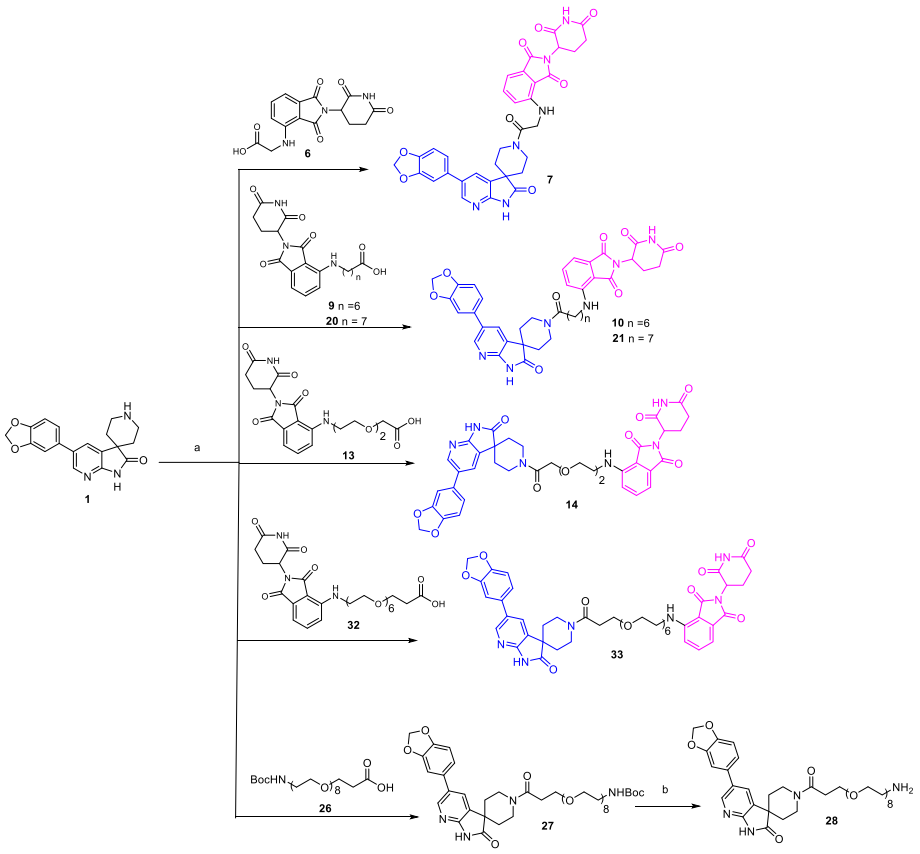

Scheme 2. Reaction conditions: a) HATU, DIPEA, DMF, RT, 2 h. b), TFA, DCM, RT, 16 h.

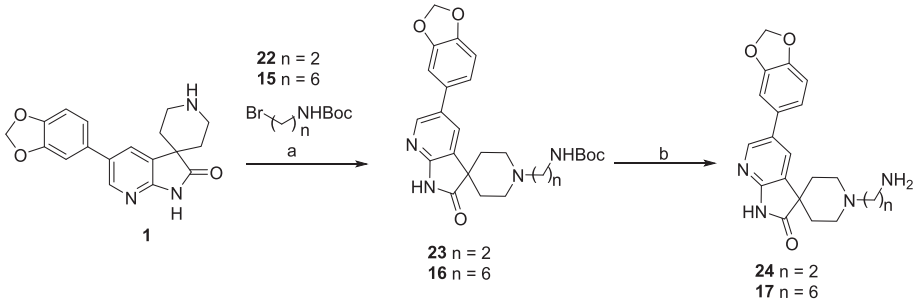

Scheme 3. Reaction conditions: a) K_2CO_3, DMF, RT, 16 h. b), TFA, DCM, RT, 16 h.

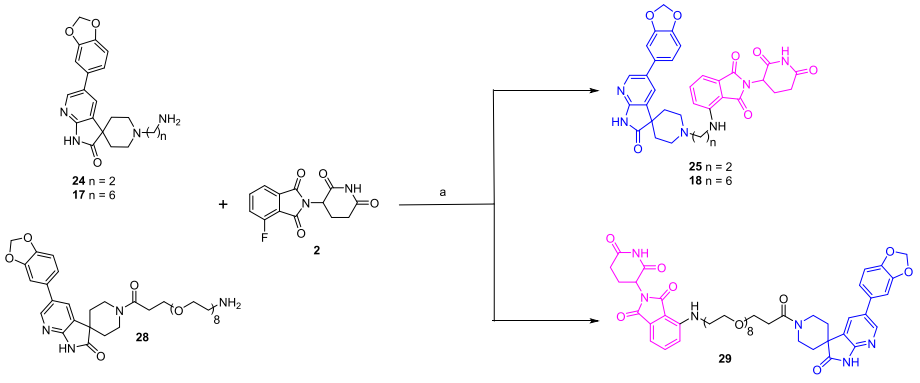

Scheme 4. Reaction condition: a) DMSO, DIPEA, 100 °C, 1 h.

Table 1
Docking scores and amino acid interactions of azaspirooxindolinone derivatives with BTK.

PROTAC	Docking score	Amino acid interactions
3	−11.5	Lys558, Tyr551, Asp521, Asn526, Gln412, Gly411, Leu408, Ser538, Val458, Meta449, Leu542- van der Waals; Arg525, Thr474- carbon hydrogen bond; Asp539- pi anion; Val416, Ala428, Lys430, Ile472, Leu460, Cys481- pi alkyl; Leu528- pi sigma; Phe540- pi-pi T-shaped
7	−12.1	Tyr551, Gly411, Gln412, Asp512, Leu408, Ser538, Leu542, Met449, Asn526, Val458, Leu408- van der Waals; Lys558, Arg525- conventional hydrogen bond; Asp539, Thr474- carbon hydrogen bond; Leu528- pi sigma; Phe540- pi-pi T-shaped; Val416, Ala428, Lys430, Ile472, Leu460- pi-alkyl
10	−10.9	Ile472, Thr474, Glu475, Val458, Tyr476, Met477, Gly480, Gly409, Trp563, Asn603, Thr410, Pro560, Phe559, Cys481, Arg525, Asp521, Gln412, Asn526, Leu542- van der Waals; Lys430, Asp539, Ser538, Lys558- conventional hydrogen bonds; Val416- pi sigma; Tyr551- pi T-shaped; Ala428, Leu528- pi alkyl
14	−11.2	Met477, Tyr476, Ser538, Val458, Ile472, Lys430, Asp539, Cys481, Gly409, Thr410, Gly480, Gly411, Asn526, Gln412, Ser543, Pro560, Trp563, Asn603, Asn562- van der Waals; Thr474, Asp521- conventional hydrogen bond; Leu408, Lys558- carbon hydrogen bond; Glu475- unfavorable donor; Arg525- pi anion; Val416- pi sigma; Tyr550- pi-pi T-shaped; Ala428, Leu528- pi alkyl
18	−11.1	Thr474, Val458, Gly411, Ser538, Met477, Tyr476, Gly480, Gly409, Asn526, Leu483- van der Waals; Lys430, Leu408, Arg525- conventional hydrogen bonds; Asn484- carbon hydrogen bonds; Asp539- pi anion; Ile472, Ala428, Val416, Leu528, Cys481- pi alkyl
21	−11.4	Asn526, Thr474, Val458, Tyr476, Ala478, Gly480, Ser538, Leu408, Thr410, Leu483, Gly411- van der Waals; Met477, Lys430, Cys481, Asn484- conventional hydrogen bond; Glu475, Gly411, Gly409- carbon hydrogen bonds; Asp539- pi anion; Ile472, Val416, Leu528, Ala428, Arg525- pi alkyl
25	−11.2	Leu408, Tyr551, Gln412, Phe413, Leu542, Gly411, Cys481, Ser538, Phe540, Met449- van der Waals; Asp521, Asn526, Arg525- conventional hydrogen bonds; Lys430- unfavorable donor; Thr474- carbon hydrogen bonds; Asp539- pi anion; Leu528- pi sigma; Ile472, Val458, Leu460, Val416, Ala428- pi alkyl
29	−8.4	Met477, Tyr551, Ser538- conventional hydrogen bonds; Lys558, Gly411, Leu435- carbo hydrogen bonds; Asp539, Lys435- pi anion; Leu528, Ile432, Val416, Ala428- pi alkyl
33	−10.7	Asp521, Phe419, Lys558, Trp563, Met596, Leu483, Thr410, Cys481, Gly409, Ser538, Val458, Glu475, Tyr476, Ala478, Asn484- van der Waals; Arg525, Met477- conventional hydrogen bonds; Asn526, Gly411, Gly480- carbon hydrogen bond; Asp539, Lys430- pi anion; Thr474, Leu528- pi Sulphur; Asp539, Lys430- pi anion, Tyr551- pi-pi T-shaped; Leu408, Val416, Ala428, Ile472- pi alkyl

moiety (**1**), the PROTAC **7** was generated that showed high cytotoxic activity against ITK- and BTK-positive cell lines with IC_{50} values in the sub-micromolar range (Table 2). Further modifications, increasing the linker length to a 6-methylene chain (PROTAC **10**) and a 7-methylene chain (PROTAC **21**), surprisingly led to a loss of anticancer activity.

Changing the linker to alkyl chains resulted in **18** (6-Methylene) and **25** (2-Methylene), with slight variation in their cytotoxicity in BTK/ITK-positive cell lines (Table 2). Notably, compared to the parental azaspirooxindolinone (PT-II-12), which demonstrated moderate cytotoxicity in BTK-positive RAMOS cells (IC_{50} = 16.4 μM) [16], the PROTAC strategy significantly enhanced the activity of PROTAC **25** in RAMOS cells (IC_{50} = 9.79 μM). This improvement suggests a possible advantage of the PROTAC approach, which enables targeted protein degradation over the inhibition mechanism of the parental compound (see next sections for evidence supporting BTK degradation).

Using an amino-PEG2-acetic acid linker resulted in **14**, resulting in increased cytotoxicity in RAMOS cells (0.54 ± 0.14 μM) than in Jurkat cells (48 ± 3.41 μM). Interestingly, **14** was highly cytotoxic to the other ITK cell line, CCRF-CEM (0.38 ± 0.08 μM).

Longer chain PEG8 and PEG6 linkers (PROTACs **29** and **33**) produced weak-moderate cytotoxicity against BTK/ITK cell lines. In contrast, **3** without a linker showed no cytotoxic effects in any of the tested BTK/ITK cell lines. Of all derivatives, only **18** showed moderate cytotoxicity against ITK/BTK null cell lines, specifically A549 (32.70 ± 6.60 μM), HCT116 (22.46 ± 3.34 μM), and U2OS (22.41 ± 5.32 μM), possibly suggesting off-target activity.

None of the active derivatives had cytotoxicity against non-cancerous fibroblasts (Table 2) or normal resting or mitogen-activated T/B-cell lymphocytes (**Table S1**). Overall, incorporating PROTAC technology substantially enhanced the cytotoxic activity of our previously synthesized azaspirooxindolinone derivatives [16].

2.4. PROTAC 25 selectively degrades BTK and inhibits its kinase activity

We selected PROTACs **7**, **14**, and **25** based on their docking scores and cytotoxicity profile to evaluate their BTK-degrading potential (Fig. 3a). RAMOS cells were treated with 0–20 μM of each compound, and BTK protein levels in whole-cell lysates were evaluated by western blotting. PROTAC **7** induced weak BTK degradation, with a maximum degradation (Dmax) of 49.70 ± 0.40 % and a half-maximal degradation concentration (DC50) of 1.29 ± 0.17 μM (Fig. 3b, c). In contrast, PROTAC **14,** despite its high cytotoxicity in RAMOS cells, failed to induce BTK degradation (Fig. 3c). Since BTK levels remained above 50 % at all tested concentrations, a DC50 value could not be determined and is reported as DC50 > 20 μM, confirming that PROTAC **14** lacks efficient BTK degradation activity. Among the three compounds, PROTAC **25** demonstrated the strongest BTK degradation, achieving a Dmax of 72.84 ± 2.81 %, indicating high degradation efficiency, and a DC50 of 0.27 ± 0.02 μM, suggesting a moderate potency (Fig. 3b, c).

To determine whether PROTAC **25**-mediated BTK degradation results in functional inhibition, we performed an in vitro kinase assay. PROTAC **25** inhibited BTK enzymatic activity with an IC50 of 0.44 ± 0.16 μM, while its inhibition of ITK was weaker, with an IC50 of 2.16 ± 0.46 μM (Fig. 3d), demonstrating BTK selectivity. Notably, PROTAC **25** did not reduce ITK protein levels in JURKAT cells, even when tested at cytotoxic or twofold higher concentrations (Fig. 3e). As expected, ibrutinib potently inhibited both BTK and ITK at nanomolar to sub-nanomolar concentrations (**Fig. S1**), consistent with its known dual-inhibitory profile.

Finally, to further validate the mechanism of BTK degradation, RAMOS cells were co-treated with PROTAC **25** and the proteasome inhibitor bortezomib (BTZ). BTZ completely blocked PROTAC **25**-mediated BTK degradation, confirming that BTK loss is proteasome-dependent (Fig. 3f).

These findings collectively establish PROTAC **25** as a potent and selective BTK degrader that functions through proteasome-dependent degradation with no detectable effect on ITK.

2.5. PROTAC 25-mediated BTK degradation suppresses downstream signaling

BTK phosphorylation and activation of the BCR signaling cascade in RAMOS cells occur following anti-IgM or lipopolysaccharide (LPS) stimulation, leading to MAPK signaling activation [22,25–27]. To determine whether PROTAC **25**-mediated BTK degradation inhibits downstream signaling, RAMOS cells were pre-treated with PROTAC **25** for 24 h, followed by anti-human IgM antibody or LPS stimulation for 10 min.

BTK phosphorylation at Tyr551 and Tyr223 was significantly reduced in treated cells, along with a reduction in p38 phosphorylation

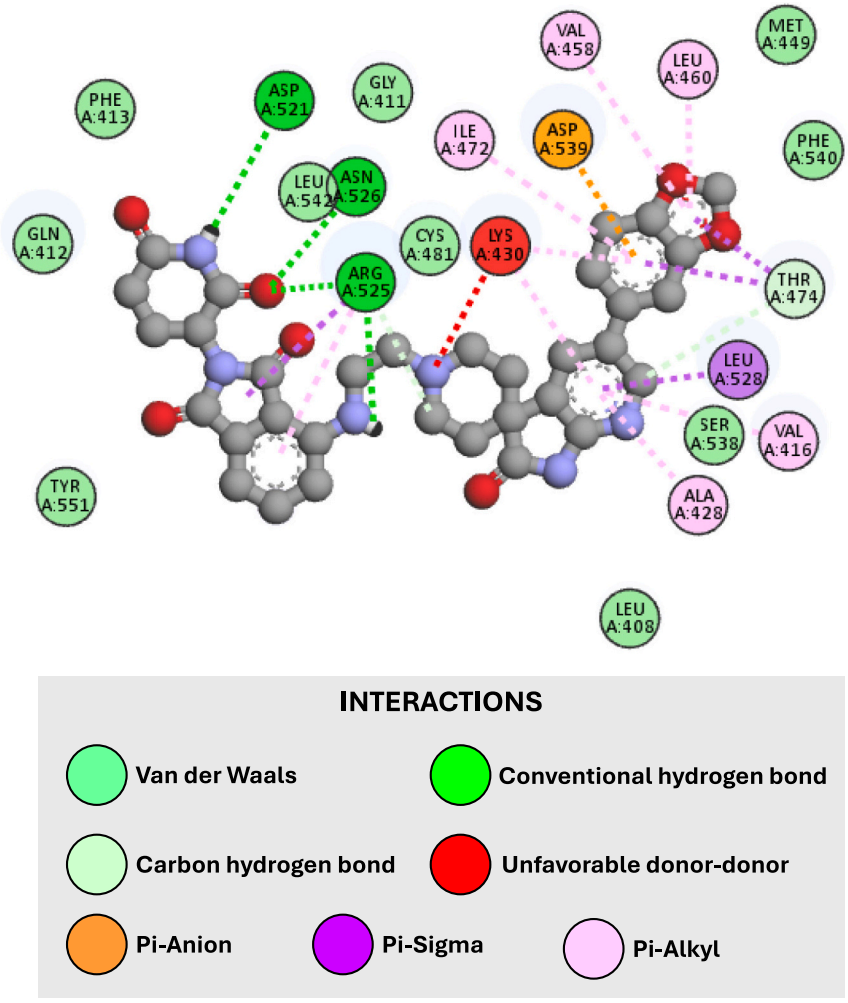

Fig. 2. Ligand interaction diagram for PROTAC 25. The diagram illustrates the binding interactions of PROTAC **25** with the BTK protein, highlighting key residues involved in the interactions. PROTAC **25** forms unique conventional hydrogen bonds with Asp521 and Asn526, which are highlighted by the darkest shade of green. These interactions were not observed together in other PROTACs tested in this study. (For interpretation of the references to colour in this figure legend, the reader is referred to the web version of this article.)

Table 2
IC_{50} values of PROTACs in μM. Data are presented as Mean ± SD, n ≥ 6 for cell lines. Representative IC_{50} curves of compounds are shown in the supplementary information.

	PROTAC								
Cell line (Cancer type, sex, ITK/BTK status)	**3**	**7**	**10**	**14**	**18**	**21**	**25**	**29**	**33**
A549 (lung adenocarcinoma, ♂, ITK/BTK null)	>50	>50	>50	>50	32.70 ± 6.60	>50	>50	>50	>50
HCT116 (colorectal carcinoma, ♂, ITK/BTK null)	>50	>50	>50	>50	22.46 ± 3.34	>50	>50	>50	>50
U2OS (osteosarcoma, ♀, ITK/BTK null)	>50	>50	>50	>50	22.41 ± 5.32	>50	>50	>50	>50
JURKAT (T-cell leukemia, ♂, ITK positive)	>50	0.73 ± 0.13	>50	> 50	3.52 ± 0.32	>50	3.42 ± 0.57	42.00 ± 3.82	39.23 ± 1.31
CCRF-CEM (T-cell leukemia, ♀, ITK positive)	>50	0.25 ± 0.03	>50	0.38 ± 0.08	2.43 ± 0.28	>50	3.81 ± 0.75	35.43 ± 6.89	35.68 ± 3.19
RAMOS (B-cell lymphoma, ♂, BTK positive)	>50	0.13 ± 0.03	>50	0.48 ± 0.06	1.27 ± 0.35	>50	9.79 ± 3.39	26.95 ± 3.99	23.54 ± 4.36
K562 (myeloid leukemia, ♀, BTK positive)	>50	>50	>50	>50	>50	>50	>50	>50	>50
MRC-5 (Normal lung fibroblast, ♂, ITK/BTK null)	>50	>50	>50	>50	>50	>50	>50	>50	>50
BJ (Normal skin fibroblast, ♂, ITK/BTK null)	>50	>50	>50	>50	>50	>50	>50	>50	>50

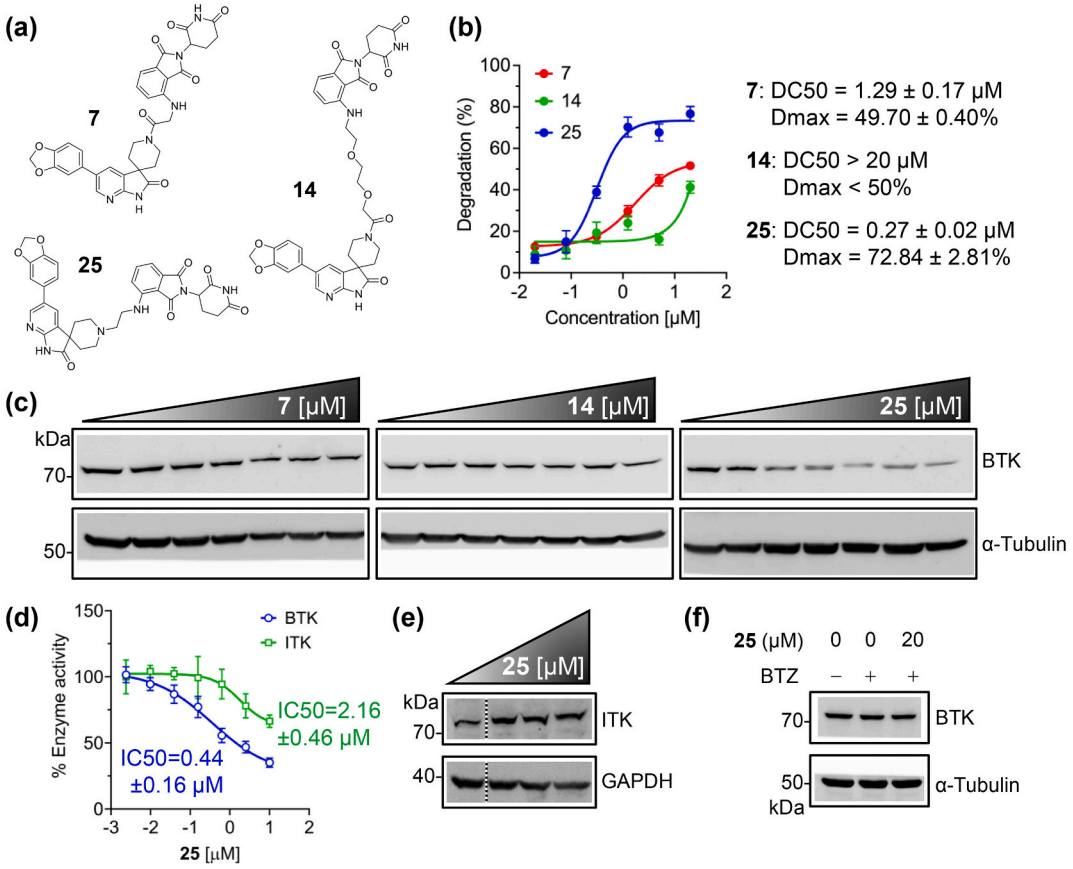

Fig. 3. PROTAC 25 selectively degrades BTK and Inhibits Enzymatic Activity. (**a**) Chemical structures of PROTAC **7**, **14**, and **25**. (**b**) Dose-response curves and corresponding DC50 and Dmax values for the three PROTACs in RAMOS cells treated at 0–20 μM after 24 h. Control cells (0 μM) were treated with 0.02 % DMSO, matching the DMSO percentage at 20 μM. DC50 and Dmax values represent the average of two independent replicates in duplicate ($n = 4$). Dose-response curves were fitted using a 4PL model ($R^2 > 0.95$) and are presented as mean ± SEM. (**c**) Western blot analysis of BTK levels in RAMOS cells treated with **7**, **14**, and **25** for 24 h. (**d**) Dose-response curves of PROTAC **25** on BTK and ITK enzyme activity. Curves were fitted using a 4PL model ($R^2 > 0.95$). Mean ± SEM ($n = 3$). (**e**) Western blot analysis of ITK levels in JURKAT cells treated with PROTAC **25** at 0, 5, 10, and 20 μM for 24 h. Dotted vertical lines indicate lane rearrangement. (**f**) Representative blot showing bortezomib (BTZ) treatment blocks PROTAC **25**-mediated BTK degradation in RAMOS cells ($n = 3$). Full blot images of panels (c), (e), and (f) are provided in the Supplementary Material.

(p-p38 Thr180/Tyr182) compared to untreated cells (Fig. 4a-d). Since Tyr551 phosphorylation by Scr-family kinases initiates BTK activation and Tyr223 autophosphorylation stabilizes its active conformation [28], their reduction by PROTAC **25** suggests that it prevents BTK activation and sustained signaling. This selective activity is likely due to the effective binding of PROTAC **25** to key BTK residues (Asp521 and Asn526), similar to the BTK inhibitor remibrutinib [21]. Overall, these findings demonstrate that PROTAC **25** efficiently degrades BTK and suppresses its downstream signaling, disrupting BCR-driven signaling pathways.

3. Conclusion

We synthesized nine azaspirooxindolinone-based PROTAC derivatives to enhance BTK-selective degradation and cytotoxic activity in BTK-positive cancer cell lines. Compared to the parent azaspirooxindolinone (PT-II-12), the PROTAC approach significantly improved potency while maintaining selectively, with no detectable toxicity in non-cancer fibroblasts or primary T- or B-cells. Among the synthesized compounds, PROTAC **25** emerged as the most effective degrader with a Dmax of ~73 % and a DC50 of 0.27 ± 0.02 μM. Mechanistically, PROTAC **25** degraded BTK in a proteasome-dependent manner and inhibited its kinase activity selectively over ITK, demonstrating preferential BTK targeting. Its enhanced activity is attributed to its strong binding to key BTK residues, similar to the BTK inhibitor remibrutinib [21]. While this study focuses on the BTK degradation efficacy of PROTAC **25**, its potential effects on CRBN neosubstrates, such as IKZF1/3, remain unexplored. Additionally, the in vivo pharmacokinetics, bioavailability, and potential toxicity of PROTAC **25** require further evaluation. Future efforts will focus on systematic SAR studies, including linker modifications and selectivity profiling, to develop optimized PROTACs with enhanced BTK degradation potency and selectivity, which will then be evaluated for in vivo efficacy and safety in preclinical models to determine their therapeutic potential. Nonetheless, our findings highlight the potential of azaspirooxindolinone-based PROTACs as targeted therapeutics for BTK-driven diseases, including hematological malignancies, autoimmune disorders, and neuroinflammation.

4. Experimental

4.1. Materials and physical measurements

All chemicals were purchased from Lancaster (Alfa Aesar, Johnson Matthey Co, Ward Hill, MA, USA), Sigma-Aldrich (St Louis, MO, USA), and Spectrochem Pvt. Ltd. (Mumbai, India). Amino acids and amino acid esters were procured from Combi-Blocks, Inc. (San Diego, USA) and BLD Pharm (India). Reactions were monitored by TLC on aluminum plates coated with silica gel and a fluorescent indicator (F254S). Visualization was achieved using UV light, $KMnO_4$ strain, and iodine indicator.

^1H NMR and ^{13}C NMR spectra were recorded on Bruker 400 MHz

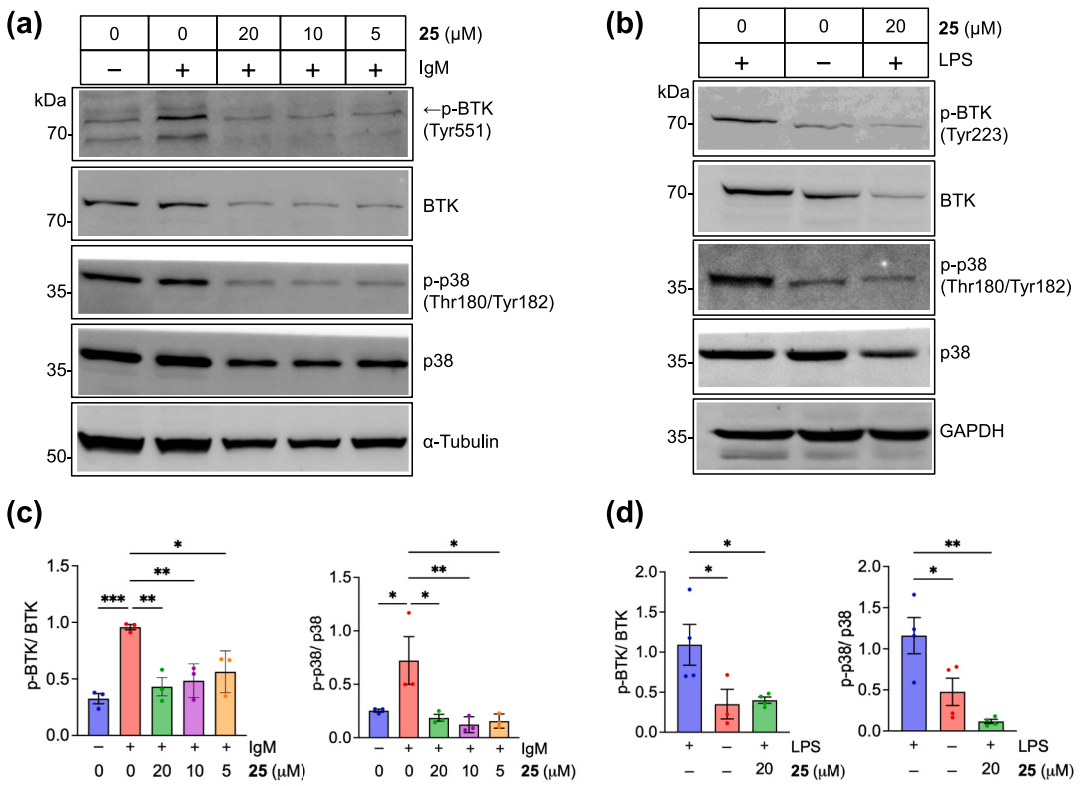

Fig. 4. PROTAC 25-mediated BTK degradation suppresses downstream signaling. (**a, b**) Western blots of BTK and p38 phosphorylation in Ramos cells pre-treated with PROTAC **25**, followed by IgM (**a**) or LPS (**c**) stimulation. Full blot images for panels are provided in the Supplementary Material. (**c, d**) Quantification of p-BTK/BTK and p-p38/p38 ratios for IgM (**c**) and LPS (**d**) stimulation. Mean ± SEM ($n = 3$ for IgM; $n = 2$ for LPS). $^{*}P < 0.05$, $^{**}P < 0.01$, $^{***}P < 0.001$, one-way ANOVA (Dunnett's test).

NMR Magnet (Billerica, Massachusetts, USA). Chemical shifts were reported in ppm, downfield from internal TMS standard. Spectral patterns are designated as follows: s (singlet), d (doublet), dd (doublet of doublets), t (triplet), td (triplet of doublets), bs (broad singlet), m (multiplet). ESI spectra were recorded on a Microaass Quattro LC using ESI+ software, a capillary voltage of 3.98 kV, and a positive ion trap detector. IR spectra were recorded on an FT-IR spectrometer, with only major peaks reported in cm^{-1}. All solutions were prepared in deionized distilled water. All other reagents were of standard quality and commercially available.

4.2. Chemistry

4.2.1. General procedure for amide coupling

To a solution of amine (1.0 equiv.) in DMF (10 v) at 0 °C under a nitrogen atmosphere, the acid (1.2 equiv.), HATU (1.5 equiv.) and diisopropylethylamine (DIPEA) (3 equiv.) were subsequently added. The reaction mixture was stirred at room temperature for 2 h, with the progress monitored by TLC. After completion, the reaction mixture was diluted with 5 mL water and extracted with ethyl acetate (3 × 10 mL). The combined organic layers were washed with brine (2 × 10 mL), dried over sodium sulfate, and concentrated under reduced pressure to yield the crude product. The crude product was first purified using normal-phase chromatography on a 12 g silica cartridge (REVELERIS) with 2–5 % methanol in DCM. Further purification was performed using reverse-phase C18 chromatography on a 12 g C18 cartridge (REVELERIS), with a gradient of 30–40 % acetonitrile in 0.1 % in formic acid-water. The purified fraction was lyophilized to yield the final product as a solid.

4.2.2. General procedure for substitution reaction

To a solution of 2-(2,6-dioxopiperidin-3-yl)-4-fluoroisoindoline-1,3-dione (1 equiv.) in DMSO (10 v) at room temperature, amine (1.2 equiv.) and DIPEA (3 equiv.) were added in a sealed tube. The reaction mixture was stirred at 100 °C for 1 h, with progress monitored by TLC. Upon completion, the reaction mixture was poured into 5 mL water and extracted with ethyl acetate (3 × 10 mL). The combined organic layers were washed with brine (2 × 10 mL), dried over sodium sulfate, and concentrated under reduced pressure to obtain the crude product. The crude product was purified using GRACE normal-phase chromatography on a 12 g silica cartridge (REVELERIS) with a gradient of 50–100 % ethyl acetate in petroleum ether, yielding the final product.

4.2.3. General procedure for global de-protection of Boc and tertiary butyl ester groups

To a solution of Boc-protected amine or tertiary butyl ester in dry DCM (10 v) at 0 °C, trifluoroacetic acid (TFA, 5.0 equiv.) was added dropwise. The reaction mixture was stirred at room temperature for 16 h, with progress monitored by TLC. Upon completion, the reaction mixture was concentrated under reduced pressure to remove volatiles. The residue was co-distilled with diethyl ether to afford the TFA salt of the product. This TFA salt was used directly in the next step without further purification.

4.2.4. General procedure for N-alkylation reaction

To a solution of amine (1 equiv.) in DMF (10 v) at room temperature, the bromo derivative (1.2 equiv.) and potassium carbonate (1.5 equiv.) were added. The reaction mixture was stirred at room temperature for 16 h, with progress monitored by TLC. Upon completion, the reaction mixture was poured into water (5 mL) and extracted with ethyl acetate (3 × 10 mL). The combined organic layers were washed with brine (2 × 5 mL), dried over sodium sulfate, and concentrated under reduced pressure to obtain the crude product. The crude product was purified using Biotage chromatography on a 12 g silica cartridge (REVELERIS),

with elution using a gradient of 2–5 % methanol in DCM, to afford the final product.

4.2.4.1. Procedure for 5′-(benzo[d][1,3]dioxol-5-yl)spiro[piperidine-4,3′-pyrrolo[2,3-b]pyridin]-2′(1′H)-one (compound 1). Compound **1** was synthesized following the previously reported procedure [29].

4.2.4.2. Procedure for 2-(2,6-dioxopiperidin-3-yl)-4-fluoroisoindoline-1,3-dione (compound 2). A mixture of 4-fluoroisobenzofuran-1,3-dione (2 g, 12.19 mmol), 3-aminopiperidine-2,6-dione hydrochloride (2.02 g, 12.19 mmol), and sodium acetate (1.5 g, 18.29 mmol) in acetic acid (20 mL) was stirred at 135 °C for 16 h. After completion, the reaction mixture was cooled to room temperature and concentrated under reduced pressure. The resulting residue was suspended in water (100 mL) and stirred at room temperature for 2 h. The precipitated solid was collected by filtration, washed, and dried under vacuum to afford 2-(2,6-dioxopiperidin-3-yl)-4-fluoroisoindoline-1,3-dione (**2**) as a beige solid (3.0 g, 91 % yield).

MS $(M+H)^+ : m/z = 277.25$.

This compound (**2**) was synthesized following a previously reported procedure[30].

4.2.4.3. ***Procedure for (4-(5′-(benzo[d][1,3]dioxol-5-yl)-2′-oxo-1′,2′-dihydrospiro[piperidine-4,3′-pyrrolo[2,3-b]pyridin]-1-yl)-2-(2,6-dioxopiperidin-3-yl)isoindoline-1,3-dione*** *(compound **3**).* To a solution of 2-(2,6-dioxopiperidin-3-yl)-4-fluoroisoindoline-1,3-dione (**2**) (42.7 mg, 0.154 mmol, 1.0 equiv.) and 5′-(benzo[d][1,3]dioxol-5-yl)spiro [piperidine-4,3′-pyrrolo[2,3-*b*]pyridin]-2′(1′H)-one (**1**) (50 mg, 0.154 mmol, 1.0 equiv.) in DMSO (0.5 mL), DIPEA (0.08 mL, 0.467 mmol, 3 equiv.) was added. The reaction mixture was stirred at 100 °C for 1 h, with the progress monitored by TLC and LC-MS. Upon completion, the reaction mixture was cooled to room temperature, diluted with ethyl acetate (10 mL), and washed with water (3 × 5 mL). The organic layer was separated, washed with brine, dried over sodium sulfate, filtered, and concentrated under reduced pressure to yield the crude product. The crude product was purified twice using GRACE reverse-phase chromatography on a 12 g C18 silica cartridge (REVELERIS), eluted with a gradient of 20–30 % acetonitrile in 0.1 % formic acid in water. The purified fractions were lyophilized to yield 4-(5′-(benzo[d][1,3] dioxol-5-yl)-2′-oxo-1′,2′-dihydrospiro[piperidine-4,3′-pyrrolo[2,3-*b*]pyridin]-1-yl)-2-(2,6-dioxopiperidin-3-yl)isoindoline-1,3-dione (**3**) (10 mg, 10 %) as a pale yellow solid.

^{1}H NMR (400 MHz, DMSO-d_6)*:** δ 11.15 (s, 1H), 11.08 (s, 1H), 8.34 (m, 1H), 8.14 (s, 1H), 7.73 (t, $J = 7.6$ Hz, 1H), 7.47 (d, $J = 8.4$ Hz, 1H), 7.38–7.33 (m, 2H), 7.18 (d, $J = 8.0$ Hz, 1H), 6.99 (d, $J = 8.0$ Hz, 1H), 6.05 (s, 2H), 5.13–5.08 (m, 1H), 3.74–3.62 (m, 4H), 2.89–2.87 (m, 1H), 2.67–2.55 (m, 2H), 2.05–2.02 (m, 5H); ***^{13}C NMR (400 MHz, DMSO-d_6): 180.5, 172.7, 170.0, 167.3, 166.3, 155.0, 150.0, 147.9, 146.7, 144.1, 135.7, 133.6, 131.6, 129.9, 129.6, 128.5, 124.2, 120.1, 116.3, 114.6, 108.6, 107.1, 101.0, 69.7, 48.7, 46.2, 46.1, 45.0. 31.9, 30.9, 22.0. ***LC-MS (ES-API)*:** $m/z = 580.1$ $(M + H)^+$.

4.2.4.4. ***Preparation of tert-butyl (2-(2,6-dioxopiperidin-3-yl)-1,3-dioxoisoindolin-4-yl)glycinate*** *(compound **5**).* To a solution of 2-(2,6-dioxopiperidin-3-yl)-4-fluoroisoindoline-1,3-dione (2) (50 mg, 0.181 mmol, 1.0 equiv.) and tert-butyl glycine (4) (28 mg, 0.217 mmol, 1.2 equiv.) in DMSO (0.5 mL), DIPEA (0.1 mL, 0.543 mmol, 3.0 equiv.) was added at room temperature. The reaction mixture was stirred at 100 °C for 1 h and monitored by TLC and LC-MS. Upon completion of the reaction, the mixture was cooled, diluted with water (10 mL), and extracted with ethyl acetate (3 × 15 mL). The combined organic layers were washed with water and brine, dried over sodium sulfate, filtered, and concentrated under reduced pressure to yield the crude product. The crude product was purified by GRACE normal-phase chromatography on a 12 g silica cartridge (REVELERIS), using a gradient of 40–50 % ethyl acetate in petroleum ether. The purified product was obtained as a pale yellow foamy solid (64 mg, 64 % yield) and identified as tert-butyl (2-(2,6-dioxopiperidin-3-yl)-1,3-dioxoisoindolin-4-yl)glycinate (**5**).

^{1}H NMR (400 MHz, $CDCl_3$): δ 7.95 (bs, 1H), 7.51 (t, $J = 8.0$ Hz, 1H), 7.16 (d, $J = 7.2$ Hz, 1H), 6.77–6.71 (m, 2H), 4.94–4.90 (m, 1H), 3.98 (d, $J = 6.0$ Hz, 2H), 2.98–2.61 (m, 3H), 2.14–2.11 (m, 1H), 1.50 (m, 9H); ***LC-MS (ES-API)***: $m/z = 388.2$ $(M + H)^+$.

4.2.4.5. ***Preparation of (2-(2,6-dioxopiperidin-3-yl)-1,3-dioxoisoindolin-4-yl)glycine*** *(compound **6**).* To a solution of tert-butyl (2-(2,6-dioxopiperidin-3-yl)-1,3-dioxoisoindolin-4-yl)glycinate (**5**) (100 mg, 0.258 mmol, 1.0 equiv.) in DCM (1 mL) at 0 °C, trifluoroacetic acid (TFA, 0.147 mL, 1.291 mmol, 5.0 equiv.) was added dropwise. The reaction mixture was stirred at room temperature for 16 h, with progress monitored by TLC and LC-MS. Upon completion, the reaction mixture was concentrated under reduced pressure and co-distilled with diethyl ether to yield the crude product, (2-(2,6-dioxopiperidin-3-yl)-1,3-dioxoisoindolin-4-yl)glycine (**6**) (100 mg), as a pale-yellow viscous liquid. This crude product was used directly in the next step without further purification.

LC-MS (ES-API): $m/z = 332.5$ $(M + H)^+$, consistent with the previously reported data [31].

4.2.4.6. ***Preparation of 4-((2-(5′-(benzo[d][1,3]dioxol-5-1yl)-2′-oxo-1′,2′-dihydrospiro[piperidine-4,3′-pyrrolo[2,3-b]pyridin]-1-yl)-2-oxoethyl)amino)-2-(2,6-dioxopiperidin-3-yl)isoindoline-1,3-dione*** *(compound **7**).* To a stirred solution of 5′-(benzo[d][1,3]dioxol-5-yl) spiro[piperidine-4,3′-pyrrolo[2,3-*b*]pyridin]-2′(1′H)-one (**1**) (100 mg, 0.309 mmol, 1.0 equiv.) in DMF (1 mL) at 0 °C under a nitrogen atmosphere, (2-(2,6-dioxopiperidin-3-yl)-1,3-dioxoisoindolin-4-yl) glycine (**6**) (100 mg, 0.309 mmol, 1.0 equiv.), HATU (172 mg, 0.465 mmol, 1.5 equiv.) and DIPEA (0.26 mL, 1.54 mmol, 5.0 equiv.) were added. The reaction mixture was stirred at room temperature for 2 h, with progress monitored by TLC. After completion, the mixture was diluted with water (5 mL) and extracted with ethyl acetate (3 × 15 mL). The combined organic layers were washed with brine (2 × 10 mL), dried over sodium sulfate, and concentrated under reduced pressure to afford the crude product. Purification was performed twice using GRACE reverse-phase chromatography on a 12 g C18 silica cartridge (REVELERIS) with a 35–40 % acetonitrile gradient in 0.1 % formic acid/water. The collected fractions were lyophilized to yield 4-((2-(5′-(benzo [d][1,3]dioxol-5-yl)-2′-oxo-1′,2′-dihydrospiro[piperidine-4,3′-pyrrolo [2,3-*b*]pyridin]-1-yl)-2-oxoethyl)amino)-2-(2,6-dioxopiperidin-3-yl)isoindoline-1,3-dione (**7**) as a pale-yellow solid (40 mg, 21 % yield).

^{1}H NMR (500 MHz, DMSO-d_6): δ 11.17 (bs, 1H), 11.08 (s, 1H), 8.34 (s, 1H), 8.10 (s, 1H), 7.62 (t, $J = 8.0$ Hz, 1H), 7.31 (s, 1H), 7.18–7.16 (m, 3H), 7.08 (d, $J = 7.0$ Hz, 1H), 6.98 (d, $J = 8.0$ Hz, 1H), 6.04 (s, 2H), 5.09–5.05 (m, 1H), 4.34–4.31 (m, 1H), 4.30–4.19 (m, 1H), 3.99–3.16 (m, 1H), 3.89–3.83 (m, 3H), 2.89–2.86 (m, 1H), 2.69–2.55 (m, 1H), 2.05–2.03 (m, 1H), 1.95–1.75 (m, 1H); ***^{13}C NMR (500 MHz, DMSO-d_6)***: 180.5, 172.8, 170.1, 168.8, 167.3, 166.4, 155.2, 147.9, 146.7, 145.3, 144.1, 136.1132.0, 131.6, 129.8, 129.5, 128.2, 119.9, 118.2, 110.7, 109.5, 108.6, 106.9, 101.1, 48.5, 45.1, 43.7, 37.3, 31.6. 31.2, 30.9, 22.15; ***LC-MS (ES-API)***: $m/z = 637.2$ $(M + H) +$. ***IR***: 1708.9 cm^{-1}(C═O stretching); ***Mp***: 215–218 °C.

4.2.4.7. ***Preparation of 7-((2-(2,6-dioxopiperidin-3-yl)-1,3-dioxoisoindolin-4-yl)amino)heptanoic acid*** *(compound **9**).* To a solution of 2-(2,6-dioxopiperidin-3-yl)-4-fluoroisoindoline-1,3-dione (**2**) (100 mg, 0.362 mmol, 1.0 equiv.) and 7-aminoheptanoic acid (**8**) (63 mg, 0.434 mmol, 1.2 equiv., BLD pharma) in DMSO (1 mL) at room temperature, DIPEA (0.31 mL, 1.81 mmol, 5 equiv.) was added. The reaction mixture was stirred at 100 °C for 1 h and monitored by TLC and LC-MS. After

completion, the reaction mixture was cooled to room temperature, diluted with water (5 mL), and extracted with ethyl acetate (3 × 10 mL). The combined organic layers were washed sequentially with water and brine and dried over sodium sulfate, filtered, and concentrated under reduced pressure to obtain the crude product. The crude product was purified by GRACE normal-phase chromatography on a 12 g silica cartridge (REVELERIS), eluted with a gradient of 5–10 % methanol in DCM, to yield 7-((2-(2,6-dioxopiperidin-3-yl)-1,3-dioxoisoindolin-4-yl)amino) heptanoic acid (**9**) as a pale yellow foamy solid (52 mg, 35 % yield) [32].

$$LC-MS\ (ES-API): m/z = 402.2\ (M+H)^{+.}$$

4.2.4.8. ***Preparation of 4-((7-(5′-(benzo[d][1,3]dioxol-5-yl)-2′-oxo-1′,2′-dihydrospiro[piperidine-4,3′-pyrrolo[2,3-b]pyridin]-1-yl)-7-oxoheptyl)amino)-2-(2,6-dioxopiperidin-3-yl)isoindoline-1,3-dione*** *(compound **10**)*. To a stirred solution of 5′-(benzo[d][1,3]dioxol-5-yl) spiro[piperidine-4,3′-pyrrolo[2,3-*b*]pyridin]-2'(1′H)-one (**1**) (40 mg, 0.123 mmol) in DMF (0.5 mL) at 0 °C under a nitrogen atmosphere, 7-((2-(2,6-dioxopiperidin-3-yl)-1,3-dioxoisoindolin-4-yl)amino)heptanoic acid (**9**) (40 mg, 0.123 mmol), HATU (70 mg, 1.84 mmol, 1.5 equiv.) and DIPEA (0.064 mL, 0.369 mmol, 3 equiv.) were added. The reaction mixture was stirred at room temperature for 2 h, with progress monitored by TLC. Upon completion, the reaction mixture was diluted with 5 mL of water and extracted with ethyl acetate (3 × 10 mL). The combined organic layers were washed with brine (2 × 10 mL), dried over sodium sulfate, filtered, and concentrated under reduced pressure to yield the crude product. Purification was performed using GRACE reverse-phase chromatography on a 12 g C18 cartridge (REVELERIS), eluting with 35–40 % acetonitrile/0.1 % formic acid in water. The collected fractions were lyophilized to yield 4-((7-(5′-(benzo[d][1,3]dioxol-5-yl)-2′-oxo-1′,2′-dihydrospiro[piperidine-4,3′-pyrrolo[2,3-*b*]pyridin]-1-yl)-7-oxo-heptyl)amino)-2-(2,6-dioxopiperidin-3-yl)isoindoline-1,3-dione (**10**) as a pale-yellow solid (25 mg, 29 %).

^{1}H NMR (400 MHz, DMSO-d_6)*:** δ 11.17 (s, 2H), 8.53 (s, 1H), 8.33 (m, 1H), 8.10 (s, 1H), 7.57 (t, J = 8.4 Hz, 1H), 7.32 (s, 1H), 7.17 (dd, J = 1.6 Hz, 8.4 Hz, 1H), 7.10 (d, J = 8.4 Hz, 1H), 7.02–6.67 (m, 2H), 6.54 (t, J = 6.4 Hz, 1H), 6.05 (s, 2H), 5.06–5.02 (m, 1H), 3.83–3.75 (m, 4H), 3.31–3.30 (m, 2H, merged with moister), 2.87–2.84 (m, 1H), 2.59–2.55 (m, 2H), 2.39–2.33 (m, 2H), 2.03–2.00 (m, 1H), 1.81–1.73 (m, 4H), 1.61–1.50 (m, 4H), 1.49–1.32 (m, 4H). ***LC-MS (ES-API): m/z = 707.2 $(M+H)^+$. ***IR***: 1701.2 cm^{-1}(C═O stretching). ***Mp***: 197–200 °C.

4.2.4.9. ***Preparation of tert-butyl 2-(2-(2-((2-(2,6-dioxopiperidin-3-yl)-1,3-dioxoisoindolin-4-yl)amino)ethoxy)ethoxy)acetate*** *(compound **12**)*. To a solution of 2-(2,6-dioxopiperidin-3-yl)-4-fluoroisoindoline-1,3-dione (**2**) (130 mg, 0.471 mmol) and compound **11** (123 mg, 0.565 mmol, 1.2 equiv., BLD Pharma) in DMSO (1.3 mL) at room temperature, DIPEA (0.25 mL, 1.41 mmol, 3.0 equiv.) was added. The reaction mixture was stirred at 100 °C for 1 h, with progress monitored by TLC and LC-MS. After completion, the reaction mixture was cooled to room temperature, diluted with 5 mL of water, and extracted with ethyl acetate (2 × 10 mL). The combined organic layers were washed sequentially with water and brine, dried over anhydrous sodium sulfate, filtered, and concentrated under reduced pressure to obtain the crude product. The crude product was purified using GRACE normal-phase chromatography on a 12 g silica cartridge (REVELERIS), with elution using a gradient of 5–10 % methanol in DCM. The purified product was obtained as tert-butyl 2-(2-(2-((2-(2,6-dioxopiperidin-3-yl)-1,3-dioxoisoindolin-4-yl)amino)ethoxy)ethoxy)acetate (**12**), a pale-yellow solid (65 mg, 29 % yield).

^{1}H NMR (400 MHz, $CDCl_3$): δ 7.92 (s, 1H), 7.50 (t, J = 8.0 Hz, 1H), 7.10 (d, J = 7.2 Hz, 1H), 6.93 (d, J = 8.4 Hz, 1H), 6.49–6.47 (m, 1H), 4.93–4.88 (m, 1H), 4.11 (s, 2H), 3.75–3.71 (m, 6H), 3.61–3.46 (m, 2H), 2.91–2.72 (m, 3H), 2.14–2.11 (m, 1H), 1.47 (m, 9H); ***LC-MS (ES-API)***: m/z = 476.2 $(M+H)^+$.

4.2.4.10. Preparation of 2-(2-(2-((2-(2,6-dioxopiperidin-3-yl)-1,3-dioxoisoindolin-4-yl)amino)ethoxy)ethoxy)acetic acid (compound 13). To a solution of tert-butyl 2-(2-(2-((2-(2,6-dioxopiperidin-3-yl)-1,3-dioxoisoindolin-4-yl)amino)ethoxy)ethoxy)acetate (**12**) (65 mg, 0.136 mmol) in DCM (1 mL) at 0 °C, trifluoroacetic acid (TFA, 0.078 mL, 0.684 mmol, 5.0 equiv.) was added dropwise. The reaction mixture was stirred at room temperature for 16 h, with progress monitored by TLC and LC-MS. Upon completion, the reaction mixture was concentrated under reduced pressure and co-distilled with diethyl ether to afford the crude product (80 mg), identified as 2-(2-(2-((2-(2,6-dioxopiperidin-3-yl)-1,3-dioxoisoindolin-4-yl)amino)ethoxy)ethoxy)acetic acid (**13**), a pale-yellow viscous liquid.

LC-MS (ES-API): m/z = 420.2 $(M+H)^+$, consistent with previously reported data [32].

4.2.4.11. ***Preparation of 4-((2-(2-(2-(5′-(benzo[d][1,3]dioxol-5-yl)-2′-oxo-1′,2′-dihydrospiro[piperidine-4,3′-pyrrolo[2,3-b]pyridin]-1-yl)-2-oxoethoxy)ethoxy)ethyl)amino)-2-(2,6-dioxopiperidin-3-yl) isoindoline-1,3-dione*** *(compound **14**)*. To a stirred solution of 5′-(benzo[d][1,3]dioxol-5-yl)spiro[piperidine-4,3′-pyrrolo[2,3-*b*]pyridin]-2'(1′H)-one (**1**) (75 mg, 0.185 mmol) in DMF (0.5 mL) at 0 °C under a nitrogen atmosphere, 2-(2-(2-((2-(2,6-dioxopiperidin-3-yl)-1,3-dioxoisoindolin-4-yl)amino)ethoxy)ethoxy)acetic acid (**13**) (60 mg, 0.185 mmol), HATU (105 mg, 0.277 mmol, 1.5 equiv.), and DIPEA (0.09 mL, 0.55 mmol, 3.0 equiv.) were added. The reaction mixture was stirred at room temperature for 2 h, with progress monitored by TLC. Upon completion, the reaction mixture was diluted with 5 mL of water and extracted with ethyl acetate (3 × 12 mL). The combined organic layers were washed with brine (2 × 10 mL), dried over anhydrous sodium sulfate, filtered, and concentrated under reduced pressure to yield the crude product. The crude product was purified twice using GRACE reverse-phase chromatography on a 12 g C18 silica cartridge (REVELERIS), with elution using a gradient of 35–40 % acetonitrile in 0.1 % formic acid in water. The collected fractions were lyophilized to yield 4-((2-(2-(2-(5′-(benzo[d][1,3]dioxol-5-yl)-2′-oxo-1′,2′-dihydrospiro[piperidine-4,3′-pyrrolo[2,3-*b*]pyridin]-1-yl)-2-oxoethoxy)ethoxy)ethyl) amino)-2-(2,6-dioxopiperidin-3-yl)isoindoline-1,3-dione (**14**) as a pale-yellow solid (20 mg, 15 % yield).

^{1}H NMR (400 MHz, DMSO-d_6): δ 11.17 (bs, 1H), 11.08 (s, 1H), 8.35 (s, 1H), 8.10 (s, 1H), 7.56 (t, J = 8.4 Hz, 1H), 7.31 (s, 1H), 7.17–7.11 (m, 2H), 7.00 (dd, J = 17.6, 8.4 Hz, 2H), 6.54 (t, J = 6.4 Hz, 1H), 6.04 (s, 2H), 5.05–5.00 (m, 1H), 4.26–4.17 (m, 2H), 3.85–3.76 (m, 3H), 3.65–3.62 (m, 7H), 3.47–3.46 (m, 2H), 2.85–2.81 (m, 1H), 2.02–1.98 (m, 2H), 1.82–1.75 (m, 4H); ***^{13}C NMR (400 MHz, DMSO-d_6)*:** 180.3, 172.7, 170.0, 168.9, 167.3, 167.2, 154.9, 147.9, 146.7, 146.3, 144.1, 136.1, 132.0, 131.5, 129.9, 129.5, 128.2, 120.0, 117.3, 110.6, 109.2, 108.6, 107.0, 101.1, 69.8, 69.5, 68.8, 48.5, 45.3, 41.7, 36.7, 31.9,31.2, 30.9, 22.1. IR: 1701.2 cm^{-1}(C═O stretching); ***LC-MS (ES-API):*** m/z = 725.3 $(M+H)^+$. ***IR:*** 1701.2 cm^{-1}(C═O stretching). ***Mp***: 167–169 °C.

4.2.4.12. ***Preparation of tert-butyl (6-(5′-(benzo[d][1,3]dioxol-5-yl)-2′-oxo-1′,2′-dihydrospiro[piperidine-4,3′-pyrrolo[2,3-b]pyridin]-1-yl) hexyl)carbamate*** *(compound **16**)*. To a solution of 5′-(benzo[d][1,3]dioxol-5-yl)spiro[piperidine-4,3′-pyrrolo[2,3-*b*]pyridin]-2'(1′H)-one (**1**) (50 mg, 0.154 mmol) and tert-butyl (6-bromohexyl)carbamate (**15**) (43 mg, 0.154 mmol, 1.0 equiv.; BLD Pharma) in DMF (1 mL) at 0 °C, potassium carbonate (42 mg, 0.308 mmol, 2.0 equiv.) was added. The reaction mixture was stirred at room temperature for 16 h, with progress monitored by TLC and LC-MS. Upon completion, the reaction mixture was diluted with 10 mL of water and extracted with ethyl acetate (2 × 15 mL). The combined organic layers were washed sequentially with water and brine, dried over anhydrous sodium sulfate, filtered, and concentrated under reduced pressure to afford the crude product. The crude product was purified using GRACE normal-phase chromatography on a 12 g silica cartridge (REVELERIS), with elution using a gradient of

2–5 % methanol in DCM, to yield tert-butyl (6-(5′-(benzo[d][1,3]dioxol-5-yl)-2′-oxo-1′,2′-dihydrospiro[piperidine-4,3′-pyrrolo[2,3-*b*]pyridin]-1-yl)hexyl)carbamate (**16**) as a pale-yellow solid (75 mg, 93 % yield).

^{1}H NMR (400 MHz, CDCl$_3$): δ 8.44 (bs, 1H), 8.27 (d, J = 2.0 Hz, 1H), 7.76 (d, J = 2.0 Hz, 1H), 6.97–6.95 (m, 2H), 6.90 (d, J = 8.0 Hz, 1H), 6.02 (s, 2H), 4.52 (m, 1H), 3.11–2.54 (m, 8H), 2.06–1.89 (m, 4H), 1.53–1.36 (m, 18H); ***LC-MS (ES-API):*** m/z = 523.3 $(M + H)^+$.

4.2.4.13. ***Preparation of 1-(6-aminohexyl)-5′-(benzo[d][1,3]dioxol-5-yl)spiro[piperidine-4,3′-pyrrolo[2,3-b]pyridin]-2′(1′H)-one*** *(compound **17**).* To a solution of tert-butyl (6-(5′-(benzo[d][1,3]dioxol-5-yl)-2′-oxo-1′,2′-dihydrospiro[piperidine-4,3′-pyrrolo[2,3-*b*]pyridin]-1-yl) hexyl)carbamate (**16**) (75 mg, 0.143 mmol) in DCM (1 mL) at 0 °C, trifluoroacetic acid (TFA, 0.08 mL, 0.718 mmol, 5.0 equiv.) was added dropwise. The reaction mixture was stirred at room temperature for 16 h, with progress monitored by TLC and LC-MS. Upon completion, the reaction mixture was concentrated under reduced pressure and co-distilled with diethyl ether to remove residual volatiles. The crude product, identified as 1-(6-aminohexyl)-5′-(benzo[d][1,3]dioxol-5-yl) spiro[piperidine-4,3′-pyrrolo[2,3-*b*]pyridin]-2′(1′H)-one TFA salt (**17**), was obtained as a pale-yellow viscous liquid (95 mg). This crude product was used directly in the subsequent step without further purification.

$\mathrm{LC-MS\ (ES-API)}: m/z = 422.1\ (M + H)^+$.

4.2.4.14. ***Preparation of 4-((6-(5′-(benzo[d][1,3]dioxol-5-yl)-2′-oxo-1′,2′-dihydrospiro[piperidine-4,3′-pyrrolo[2,3-b]pyridin]-1-yl)hexyl) amino)-2-(2,6-dioxopiperidin-3-yl)isoindoline-1,3-dione*** *(compound **18**).* To a stirred solution of 2-(2,6-dioxopiperidin-3-yl)-4-fluoroisoindoline-1,3-dione (**2**) (50 mg, 0.181 mmol) and 1-(6-aminohexyl)-5′-(benzo[d][1,3]dioxol-5-yl)spiro[piperidine-4,3′-pyrrolo[2,3-*b*]pyridin]-2′(1′H)-one TFA salt (**17**) (76 mg, 0.181 mmol, 1.0 equiv.) in DMSO (1 mL) at room temperature, DIPEA (0.16 mL, 0.90 mmol, 5.0 equiv.) was added. The reaction mixture was stirred at 100 °C for 1 h, with progress monitored by TLC and LC-MS. Upon completion, the reaction mixture was cooled to room temperature, diluted with 5 mL of water, and extracted with ethyl acetate (3 × 15 mL). The combined organic layers were washed sequentially with water and brine, dried over anhydrous sodium sulfate, filtered, and concentrated under reduced pressure to obtain the crude product. The crude product was purified using GRACE reverse-phase chromatography on a 12 g C18 silica cartridge (REVELERIS), eluting with a gradient of 25–30 % acetonitrile/0.1 % formic acid in water. The collected fractions were lyophilized to yield 4-((6-(5′-(benzo[d][1,3]dioxol-5-yl)-2′-oxo-1′,2′-dihydrospiro[piperidine-4,3′-pyrrolo[2,3-*b*]pyridin]-1-yl)hexyl)amino)-2-(2,6-dioxopiperidin-3-yl)isoindoline-1,3-dione (**18**) as a pale-yellow solid (32 mg, 25 % yield).

^{1}H NMR (400 MHz, DMSO-d$_6$): δ 11.08 (bs, 2H), 8.31 (s, 1H), 7.58 (t, J = 8.4 Hz, 1H), 7.29 (s, 1H), 7.15–7.07 (m, 2H), 7.01 (t, J = 6.8 Hz, 2H), 6.54 (t, J = 5.6 Hz, 1H), 6.06 (s, 2H), 5.06–5.02 (m, 1H), 2.92–2.83 (m, 2H), 2.56–2.55 (m, 3H), 2.03–2.00 (m, 3H), 1.95–1.73 (m, 4H), 1.60–1.49 (m, 5H), 1.42–1.32 (m, 5H), 1.23 (s, 9H), 0.85 (t, J = 5.6 Hz, 2H); ***^{13}C NMR (500 MHz, CD$_3$OD)***: 183.1, 175.4, 172.5, 171.7, 170.1, 156.9, 150.8, 149.8, 149.1, 146.6, 138.1, 134.1, 134.0, 132.1, 130.4, 122.4, 118.8, 112.6, 111.9, 110.6, 109.1, 103.5, 59.7, 44.1, 33.0, 32.9, 30.7, 28.7, 28.4, 27.1, 24.6; ***LC-MS (ES-API):*** m/z = 679.3 (M + H)+; ***IR***: 1701.2 cm^{-1}(C═O stretching); ***Mp***: 181–185 °C.

4.2.4.15. ***Preparation of 8-((2-(2,6-dioxopiperidin-3-yl)-1,3-dioxoisoindolin-4-yl)amino)octanoic acid*** *(compound **20**).* To a solution of 2-(2,6-dioxopiperidin-3-yl)-4-fluoroisoindoline-1,3-dione (**2**) (150 mg, 0.543 mmol) and 8-aminooctanoic acid (**19**) (95 mg, 0.597 mmol, 1.1 equiv., Alfa Aesar) in DMSO (1.5 mL) at room temperature, DIPEA (0.28 mL, 1.62 mmol, 3 equiv.) was added. The reaction mixture was stirred at 100 °C for 1 h, with progress monitored by TLC and LC-MS. Upon completion, the reaction mixture was cooled to room temperature, diluted with 5 mL of 1 N HCl, and extracted with ethyl acetate (3 × 10 mL). The combined organic layers were washed sequentially with water and brine, dried over anhydrous sodium sulfate, filtered, and concentrated under reduced pressure to yield the crude product. The crude product was purified using GRACE reverse-phase chromatography on a 12 g C18 silica cartridge (REVELERIS), with elution using a gradient of 50–55 % acetonitrile/0.1 % formic acid in water. The collected fractions were concentrated under reduced pressure to yield 8-((2-(2,6-dioxopiperidin-3-yl)-1,3-dioxoisoindolin-4-yl)amino)octanoic acid (**20**) as a green solid (73 mg, 33 % yield).

LC-MS (ES-API): m/z = 416.2 (M + H) +, as reported previously [33].

4.2.4.16. ***Preparation of 4-((8-(5′-(benzo[d][1,3]dioxol-5-yl)-2′-oxo-1′,2′-dihydrospiro[piperidine-4,3′-pyrrolo[2,3-b]pyridin]-1-yl)-8-oxooctyl)amino)-2-(2,6-dioxopiperidin-3-yl)isoindoline-1,3-dione*** *(compound **21**).* To a stirred solution of 5′-(benzo[d][1,3]dioxol-5-yl) spiro[piperidine-4,3′-pyrrolo[2,3-*b*]pyridin]-2′(1′H)-one (**1**) (55 mg, 0.170 mmol, 1.0 equiv.) in DMF (0.5 mL) at 0 °C under a nitrogen atmosphere, 8-((2-(2,6-dioxopiperidin-3-yl)-1,3-dioxoisoindolin-4-yl) amino)octanoic acid (**20**) (70.5 mg, 0.170 mmol, 1.0 equiv.), HATU (97 mg, 0.252 mmol, 1.5 equiv.) and DIPEA (0.08 mL, 0.51 mmol, 3.0 equiv.) were added sequentially. The reaction mixture was stirred at room temperature for 2 h, with progress monitored by TLC. Upon completion, the reaction mixture was diluted with 3 mL of water and extracted with ethyl acetate (3 × 12 mL). The combined organic layers were washed with brine, dried over anhydrous sodium sulfate, filtered, and concentrated under reduced pressure to afford the crude product.

The crude product was purified twice using GRACE reverse-phase chromatography on a 12 g C18 silica cartridge (REVELERIS), eluted with a gradient of 35–40 % acetonitrile/0.1 % ammonium bicarbonate in water. The collected fractions were lyophilized to yield 4-((8-(5′-(benzo[d][1,3]dioxol-5-yl)-2′-oxo-1′,2′-dihydrospiro[piperidine-4,3′-pyrrolo[2,3-*b*]pyridin]-1-yl)-8-oxooctyl)amino)-2-(2,6-dioxopiperidin-3-yl)isoindoline-1,3-dione (**21**) as a pale-yellow solid (10 mg, 10 % yield).

^{1}H NMR (500 MHz, CDCl$_3$): δ 8.35–8.29 (m, 2H), 8.21 (bs, 1H), 7.62 (d, J = 2.5 Hz, 1H), 7.50–7.46 (m, 1H), 7.08 (d, J = 7.0 Hz, 1H), 6.97–6.64 (m, 2H), 6.90–6.87 (m, 2H), 6.25–6.24 (m, 1H), 6.02 (s, 2H), 4.91–4.83 (m, 1H), 4.15–4.12 (m, 1H), 4.05–3.95 (m, 1H), 3.95–3.87 (m, 1H), 3.75–3.60 (m, 1H), 3.25 (q, 2H), 2.92–2.87 (m, 1H), 2.81–2.70 (m, 2H), 2.34–2.33 (m, 2H), 2.15–2.10 (m, 1H), 2.05–1.93 (m, 2H), 1.85–1.81 (m, 2H), 1.81–1.71 (m, 4H), 1.44–1.40 (m, 6H); ***^{13}C NMR (500 MHz, CD$_3$OD)***: 175.5, 175.2, 172.5, 171.7, 150.7, 149.8, 146.3, 138.0, 134.7, 134.1, 134.0, 132.2, 130.8, 122.4, 118.8, 112.5, 110.5, 109.1, 103.5, 44.2, 43.5, 39.3, 34.9, 33.9, 33.0, 31.1, 31.0, 28.6; ***LC-MS (ES-API)***: m/z = 721.5 (M + H)+; ***IR***: 1697.3 cm^{-1}(C═O stretching); ***Mp***: 162–164 °C.

4.2.4.17. ***Preparation of tert-butyl (6-(5′-(benzo[d][1,3]dioxol-5-yl)-2′-oxo-1′,2′-dihydrospiro[piperidine-4,3′-pyrrolo[2,3-b]pyridin]-1-yl) hexyl)carbamate*** *(compound **23**).* To a solution of 5′-(benzo[d][1,3] dioxol-5-yl)spiro[piperidine-4,3′-pyrrolo[2,3-*b*]pyridin]-2′(1′H)-one (**1**) (100 mg, 0.309 mmol) and tert-butyl (2-bromoethyl)carbamate (**22**) (69 mg, 0.309 mmol, 1.0 equiv., Combi) in DMF (1 mL), potassium carbonate (125 mg, 0.928 mmol, 3.0 equiv.) was added. Upon completion, the reaction mixture was diluted with 5 mL of water and extracted with ethyl acetate (2 × 12 mL). The combined organic layers were washed sequentially with water and brine, dried over anhydrous sodium sulfate, filtered, and concentrated under reduced pressure to obtain the crude product. The crude product was purified using GRACE normal-phase chromatography on a 12 g silica cartridge (REVELERIS), with elution using a gradient of 2–5 % methanol in DCM. The final product, tert-butyl (6-(5′-(benzo[d][1,3]dioxol-5-yl)-2′-oxo-1′,2′-

dihydrospiro[piperidine-4,3′-pyrrolo[2,3-*b*]pyridin]-1-yl)hexyl)carbamate (**23**), was obtained as a pale-yellow solid (53 mg, 35 % yield).

^{1}H NMR (400 MHz, CDCl$_3$): δ 8.31 (bs, 1H), 8.28 (s, 1H), 6.99–6.90 (m, 3H) 6.02 (s, 2H), 5.06 (s, 1H), 3.29 (bs, 2H), 2.97 (bs, 2H), 2.64 (m, 4H), 2.10 (bs, 2H), 1.86 (bs, 2H), 1.47 (s, 9H); ***LC-MS (ES-API)***: m/z = 467.3 $(M + H)^+$.

4.2.4.18. ***Preparation of 1-(2-aminoethyl)-5′-(benzo[d][1,3]dioxol-5-yl)spiro[piperidine-4,3′-pyrrolo[2,3-b]pyridin]-2′(1′H)-one*** *(compound **24**)*. Tert-butyl (6-(5′-(benzo[d][1,3]dioxol-5-yl)-2′-oxo-1′,2′-dihydrospiro[piperidine-4,3′-pyrrolo[2,3-*b*]pyridin]-1-yl)hexyl)carbamate (**23**) (100 mg, 0.214 mmol) was treated with trifluoroacetic acid (0.12 mL, 1.070 mmol, 5 equiv.) in DCM (1 mL) at 0 °C. The reaction mixture was stirred at room temperature for 16 h, with progress monitored by TLC and LC-MS. Upon completion, the reaction mixture was concentrated under reduced pressure and co-distilled with diethyl ether to yield 1-(2-aminoethyl)-5′-(benzo[d][1,3]dioxol-5-yl)spiro[piperidine-4,3′-pyrrolo[2,3-*b*]pyridin]-2′(1′H)-one as the TFA salt (**24**) as a pale-yellow viscous liquid (110 mg). The product was used directly in the next step without further purification.

$LC-MS\ (ES-API): m/z = 422.1\ (M + H)^+$.

4.2.4.19. ***Preparation of 4-((2-(5′-(benzo[d][1,3]dioxol-5-yl)-2′-oxo-1′,2′-dihydrospiro[piperidine-4,3′-pyrrolo[2,3-b]pyridin]-1-yl)ethyl)amino)-2-(2,6-dioxopiperidin-3-yl)isoindoline-1,3-dione*** *(compound **25**)*. To a solution of 1-(2-aminoethyl)-5′-(benzo[d][1,3]dioxol-5-yl)spiro[piperidine-4,3′-pyrrolo[2,3-*b*]pyridin]-2′(1′H)-one TFA salt (**24**) (95 mg, 0.259 mmol, 1.0 equiv.) and 2-(2,6-dioxopiperidin-3-yl)-4-fluoroisoindoline-1,3-dione (**2**) (71 mg, 0.259 mmol, 1.0 equiv.) in DMSO (1.5 mL), DIPEA (0.22 mL, 1.29 mmol, 5.0 equiv.) was added at room temperature. The reaction mixture was stirred at 100 °C for 1 h, with progress monitored by TLC and LC-MS. Upon completion, the reaction mixture was cooled to room temperature, diluted with 4 mL of water, and extracted with ethyl acetate (2 × 10 mL). The combined organic layers were washed sequentially with water and brine, dried over anhydrous sodium sulfate, filtered, and concentrated under reduced pressure to yield the crude product. The crude product was purified twice using GRACE reverse-phase chromatography on a 12 g C18 silica cartridge (REVELERIS), eluting with a gradient of 32–38 % acetonitrile/0.1 % formic acid in water. The collected fractions were lyophilized to afford 4-((2-(5′-(benzo[d][1,3]dioxol-5-yl)-2′-oxo-1′,2′-dihydrospiro[piperidine-4,3′-pyrrolo[2,3-*b*]pyridin]-1-yl)ethyl)amino)-2-(2,6-dioxopiperidin-3-yl)isoindoline-1,3-dione (**25**) as a pale-yellow solid (70 mg, 21 % yield).

^{1}H NMR (500 MHz, CDCl$_3$): δ 8.49 (bs, 2H), 8.27 (d, J = 2.0 Hz, 1H), 7.75 (d, J = 1.5 Hz, 1H), 7.51 (t, J = 8.0 Hz, 1H), 7.11 (d, J = 7.0 Hz, 1H), 6.99–6.98 (m, 2H), 6.93–6.85 (m, 1H), 6.03 (s, 2H), 4.93–4.90 (m, 1H), 3.49–3.43 (m, 2H), 3.10–3.01 (m, 2H), 2.88–2.61 (m, 8H), 2.13–2.04 (m, 5H); ***^{13}C NMR (500 MHz, DMSO-d$_6$)***: 180.6, 172.7170.0, 168.8, 167.3, 155.0, 147.9, 146.7, 146.3, 144.1, 136.2, 132.1, 131.8, 129.7, 128.7, 120.1, 117.4, 110.4, 109.2, 108.7, 107.1, 101.1, 55.9, 48.5, 47.9, 45.38, 31.9, 30.9, 22.12; ***LC-MS (ES-API)***: m/z = 623.3 (M + H)+; ***IR***: 1703.1 cm^{-1}(C═O stretching); ***Mp***: 195–199 °C.

4.2.4.20. ***Preparation of tert-butyl (27-(5′-(benzo[d][1,3]dioxol-5-yl)-2′-oxo-1′,2′-dihydrospiro[piperidine-4,3′-pyrrolo[2,3-b]pyridin]-1-yl)-27-oxo-3,6,9,12,15,18,21,24-octaoxaheptacosyl)carbamate*** *(compound **27**)*. To a stirred solution of 5′-(benzo[d][1,3]dioxol-5-yl)spiro[piperidine-4,3′-pyrrolo[2,3-*b*]pyridin]-2′(1′H)-one (**1**) (60 mg, 0.184 mmol, 1.0 equiv.) in DMF (0.6 mL) at 0 °C under a nitrogen atmosphere, 2,2-dimethyl-4-oxo-3,8,11,14,17,20,23,26,29-nonaoxa-5-azadotriacontan-32-oic acid (**26**) (100 mg, 0.184 mmol, 1.0 equiv.), HATU (104 mg, 0.276 mmol, 1.5 equiv.) and DIPEA (0.09 mL, 0.55 mmol, 3.0 equiv.) were added sequentially. The reaction mixture was stirred at room temperature for 2 h, with progress monitored by TLC. Upon completion, the reaction mixture was diluted with 4 mL of water and extracted with ethyl acetate (3 × 5 mL). The combined organic layers were washed with brine, dried over anhydrous sodium sulfate, filtered, and concentrated under reduced pressure to obtain the crude product. The crude product was purified twice using GRACE reverse-phase chromatography on a 12 g C18 silica cartridge (REVELERIS), eluted with a gradient of 25–30 % acetonitrile/0.1 % ammonium bicarbonate in water. The collected fractions were lyophilized to yield tert-butyl (27-(5′-(benzo[d][1,3]dioxol-5-yl)-2′-oxo-1′,2′-dihydrospiro[piperidine-4,3′-pyrrolo[2,3-*b*]pyridin]-1-yl)-27-oxo-3,6,9,12,15,18,21,24-octaoxaheptacosyl)carbamate (**27**) as a pale-yellow solid (55 mg, 32 % yield).

^{1}H NMR (400 MHz, CDCl$_3$): δ 8.28 (d, J = 2.0 Hz, 1H), 8.00 (bs, 1H), 7.63 (d, J = 2.0 Hz, 1H), 6.96–6.95 (m, 1H), 6.91–6.90 (m, 1H), 6.02 (s, 2H), 5.11 (bs, 1H), 4.20–4.00 (m, 2H), 3.95–3.85 (m, 4H), 3.65–3.61 (m, 30H), 3.55–3.54 (m, 3H), 1.44 (s, 9H); ***LC-MS (ES-API)***: m/z = 847.5 $(M + H)^+$.

4.2.4.21. ***Preparation of 1-(1-amino-3,6,9,12,15,18,21,24-octaoxaheptacosan-27-oyl)-5′-(benzo[d][1,3]dioxol-5-yl)spiro[piperidine-4,3′-pyrrolo[2,3-b]pyridin]-2′(1′H)-one*** *(compound **28**)*. To a stirred solution of tert-butyl (27-(5′-(benzo[d][1,3]dioxol-5-yl)-2′-oxo-1′,2′-dihydrospiro[piperidine-4,3′-pyrrolo[2,3-*b*]pyridin]-1-yl)-27-oxo-3,6,9,12,15,18,21,24-octaoxaheptacosyl)carbamate (**27**) (100 mg, 0.118 mmol, 1.0 equiv.) in DCM (1 mL), trifluoroacetic acid (TFA, 0.06 mL, 0.591 mmol, 5.0 equiv.) was added dropwise at 0 °C. The reaction mixture was stirred at room temperature for 16 h, with progress monitored by TLC and LC-MS. Upon completion, the reaction mixture was concentrated under reduced pressure and co-distilled with diethyl ether to remove residual volatiles. The crude product, identified as 1-(1-amino-3,6,9,12,15,18,21,24-octaoxaheptacosan-27-oyl)-5′-(benzo[d][1,3]dioxol-5-yl)spiro[piperidine-4,3′-pyrrolo[2,3-*b*]pyridin]-2′(1′H)-one (**28**) TFA salt, was obtained as a yellow viscous liquid (80 mg). This material was used directly in the subsequent step without further purification.

LC-MS (ES-API): m/z = 745.4 $(M + H)^+$.

4.2.4.22. ***Preparation of 4-((27-(5′-(benzo[d][1,3]dioxol-5-yl)-2′-oxo-1′,2′-dihydrospiro[piperidine-4,3′-pyrrolo[2,3-b]pyridin]-1-yl)-27-oxo-3,6,9,12,15,18,21,24-octaoxaheptacosyl)amino)-2-(2,6-dioxopiperidin-3-yl)isoindoline-1,3-dione*** *(compound **29**)*. To a solution of 2-(2,6-dioxopiperidin-3-yl)-4-fluoroisoindoline-1,3-dione (**2**) (35 mg, 0.128 mmol) and 1-(1-amino-3,6,9,12,15,18,21,24-octaoxaheptacosan-27-oyl)-5′-(benzo[d][1,3]dioxol-5-yl)spiro[piperidine-4,3′-pyrrolo[2,3-*b*]pyridin]-2′(1′H)-one (**28**) (94 mg, 0.128 mmol) in DMSO (0.5 mL), DIPEA (0.06 mL, 0.384 mmol, 3.0 equiv.) was added at room temperature. The reaction mixture was stirred at 100 °C for 1 h, with progress monitored by TLC and LC-MS. Upon completion, the reaction mixture was cooled to room temperature, diluted with 2 mL of water, and extracted with ethyl acetate (3 × 5 mL). The combined organic layers were washed sequentially with water and brine, dried over anhydrous sodium sulfate, filtered, and concentrated under reduced pressure to obtain the crude product. The crude product was purified twice using GRACE reverse-phase chromatography on a 12 g C18 cartridge (REVELERIS), eluted with a gradient of 32–35 % acetonitrile/10 mM ammonium bicarbonate in water. The collected fractions were lyophilized to yield 4-((27-(5′-(benzo[d][1,3]dioxol-5-yl)-2′-oxo-1′,2′-dihydrospiro[piperidine-4,3′-pyrrolo[2,3-*b*]pyridin]-1-yl)-27-oxo-3,6,9,12,15,18,21,24-octaoxaheptacosyl)amino)-2-(2,6-dioxopiperidin-3-yl)isoindoline-1,3-dione (**29**) as a pale-yellow solid (21 mg, 19 % yield).

^{1}H NMR (500 MHz, DMSO-d$_6$): δ 11.11 (s, 1H), 11.10 (s, 1H), 8.33 (d, J = 2.0 Hz, 1H), 8.08 (d, J = 2.0 Hz, 1H), 7.57 (t, J = 7.5 Hz, 1H), 7.31 (d, J = 1.5 Hz, 1H), 7.18–7.13 (m, 2H), 7.01 (d, J = 7.0 Hz, 1H),

6.98 (d, $J = 7.0$ Hz, 1H), 6.59 (t, $J = 5.5$ Hz, 1H), 6.02 (s, 2H), 5.06–5.02 (m, 1H), 3.87–3.75 (m, 4H), 3.67 (t, $J = 7.0$ Hz, 2H), 3.62 (t, $J = 5.5$ Hz, 2H), 3.56–3.44 (m, 32H), 2.91–2.85 (m, 1H), 2.71–2.65 (m, 1H), 2.62–2.55 (m, 2H), 2.05–1.95 (m, 1H), 1.82–1.74 (m, 4H); ***^{13}C NMR (500 MHz, CD_3OD)***: 183.4, 175.5, 173.2, 172.3, 171.5, 156.8, 150.7, 149.8, 149.0, 146.3, 138.1, 134.7, 134.1, 133.9, 132.2, 130.8, 122.4, 119.1, 112.9, 110.6, 109.1, 103.5, 72.4, 72.3, 72.2, 72.1, 71.4, 69.3, 44.1, 43.7, 39.4, 35.3, 34.6, 33.8, 33.0, 24.6; ***LC-MS (ES-API)***: m/z = 1003.8 (M + H)+; ***IR***: 1703.1 cm^{-1}(C═O stretching).

4.2.4.23. ***Preparation of tert-butyl 1-((2-(2,4-dioxotetrahydropyrimidin-1(2H)-yl)-1,3-dioxo-2,3-dihydro-1H-inden-4-yl)amino)-3,6,9,12,15,18-hexaoxahenicosan-21-oate*** *(compound **31**)*. To a solution of 2-(2,6-dioxopiperidin-3-yl)-4-fluoroisoindoline-1,3-dione (**2**) (300 mg, 1.08 mmol, 1.0 equiv.) and tert-butyl 1-amino-3,6,9,12,15,18-hexaoxahenicosan-21-oate (**30**) (467 mg, 1.08 mmol, 1.0 equiv.) in DMSO (3 mL), DIPEA (1 mL, 3.24 mmol, 3.0 equiv.) was added at room temperature. The reaction mixture was stirred at 100 °C for 1 h, with progress monitored by TLC and LC-MS. Upon completion, the reaction mixture was cooled to room temperature, diluted with 10 mL of water, and extracted with ethyl acetate (3 × 15 mL). The combined organic layers were washed sequentially with water and brine, dried over anhydrous sodium sulfate, filtered, and concentrated under reduced pressure to obtain the crude product. The crude product was purified using GRACE reverse-phase chromatography on a 12 g silica cartridge (REVELERIS), eluted with a gradient of 50–55 % acetonitrile/0.1 % formic acid in water. The fractions containing the compound were pooled and concentrated to afford tert-butyl 1-((2-(2,4-dioxotetrahydropyrimidin-1(2H)-yl)-1,3-dioxo-2,3-dihydro-1H-inden-4-yl)amino)-3,6,9,12,15,18-hexaoxahenicosan-21-oate (**31**) as a green solid (205 mg, 28 % yield).

^{1}H NMR (400 MHz, $CDCl_3$): δ 8.19 (s, 1H), 7.81–7.47 (m, 1H), 7.11 (d, $J = 7.2$ Hz, 1H), 6.92 (d, $J = 8.8$ Hz, 1H), 6.49–6.48 (m, 1H), 4.93–4.88 (m, 1H), 3.73–3.59 (m, 23H), 3.45 (q, 2H), 2.90–2.65 (m, 2H), 2.14–2.11 (m, 2H), 2.51 (t, 2H), 1.44 (s, 9H); ***LC-MS (ES-API)***: m/z = 666.3 $(M + H)^+$.

4.2.4.24. ***Preparation of 1-((2-(2,4-dioxotetrahydropyrimidin-1(2H)-yl)-1,3-dioxo-2,3-dihydro-1H-inden-4-yl)amino)-3,6,9,12,15,18-hexaoxahenicosan-21-oic acid*** *(compound **32**)*. To a solution of tert-butyl 1-((2-(2,4-dioxotetrahydropyrimidin-1(2H)-yl)-1,3-dioxo-2,3-dihydro-1H-inden-4-yl)amino)-3,6,9,12,15,18-hexaoxahenicosan-21-oate (**31**) (180 mg, 0.270 mmol, 1 equiv.) in DCM (2 mL) at 0 °C, trifluoroacetic acid (0.15 mL, 1.35 mmol, 5 equiv.) was added. The resulting reaction mixture was stirred at room temperature for 16 h, with progress monitored by TLC and LC-MS. Upon completion, the reaction mixture was concentrated under reduced pressure and co-distilled with diethyl ether to obtain 175 mg of 1-((2-(2,4-dioxotetrahydropyrimidin-1(2H)-yl)-1,3-dioxo-2,3-dihydro-1H-inden-4-yl) amino)-3,6,9,12,15,18-hexaoxahenicosan-21-oic acid (**32**) as a yellow viscous liquid. This material was used directly in the subsequent step without further purification.

LC-MS (ES-API): m/z = 610.3 $(M + H)^+$.

4.2.4.25. ***Preparation of 1-(4-((21-(5′-(benzo[d][1,3]dioxol-5-yl)-2′-oxo-1′,2′-dihydrospiro[piperidine-4,3′-pyrrolo[2,3-b]pyridin]-1-yl)-21-oxo-3,6,9,12,15,18-hexaoxahenicosyl)amino)-1,3-dioxo-2,3-dihydro-1H-inden-2-yl)dihydropyrimidine-2,4(1H,3H)-dione*** *(compound **33**)*. To a stirred solution of 5′-(benzo[d][1,3]dioxol-5-yl)spiro [piperidine-4,3′-pyrrolo[2,3-*b*]pyridin]-2'(1′H)-one (**1**) (80 mg, 0.246 mmol, 1.0 equiv.) in DMF (2 mL) at 0 °C under a nitrogen atmosphere were added 1-((2-(2,4-dioxotetrahydropyrimidin-1(2H)-yl)-1,3-dioxo-2,3-dihydro-1H-inden-4-yl)amino)-3,6,9,12,15,18-hexaoxahenicosan-21-oic acid (**32**) (150 mg, 0.246 mmol, 1.0 equiv.), HATU (140 mg, 0.369 mmol, 1.5 equiv.), and DIPEA (0.13 mL, 0.738 mmol, 3.0 equiv.). The reaction mixture was stirred at room temperature for 1 h, with progress monitored by TLC. Upon completion, the reaction mixture was diluted with 5 mL of water and extracted with ethyl acetate (3 × 10 mL). The combined organic layers were washed with brine, dried over anhydrous sodium sulfate, and concentrated under reduced pressure to obtain the crude product. The crude product was purified twice using GRACE reverse-phase chromatography on a 12 g C18 silica cartridge (REVELERIS), eluted with a gradient of 40–45 % acetonitrile/10 mM ammonium bicarbonate in water. The collected fractions were lyophilized to yield 1-(4-((21-(5′-(benzo[d][1,3]dioxol-5-yl)-2′-oxo-1′,2′-dihydrospiro[piperidine-4,3′-pyrrolo[2,3-*b*]pyridin]-1-yl)-21-oxo-3,6,9,12,15,18-hexaoxahenicosyl)amino)-1,3-dioxo-2,3-dihydro-1H-inden-2-yl)dihydropyrimidine-2,4(1H,3H)-dione (**33**) as an off-white solid (45 mg, 20 % yield).

^{1}H NMR (400 MHz, DMSO-d_6): δ 11.11 (bs, 2H), 8.33 (t, $J = 2.0$ Hz, 1H), 8.08 (d, $J = 2.0$ Hz, 1H), 7.59–7.55 (m, 1H), 7.31 (d, $J = 2.0$ Hz, 1H), 7.18–7.12 (m, 2H), 7.03 (d, $J = 7.2$ Hz, 1H), 6.98 (d, $J = 7.2$ Hz, 1H), 6.05 (s, 2H), 5.06–5.02 (m, 1H), 3.84–3.77 (m, 4H), 3.65 (t, $J = 6.4$ Hz, 1H), 3.61 (t, $J = 5.2$ Hz, 1H), 3.55–3.45 (m, 23H), 2.91–2.81 (m, 1H), 2.67–2.65 (m, 1H), 2.62–2.57 (m, 3H), 2.05–2.00 (m, 1H), 1.85–1.71 (m, 4H); ***^{13}C NMR (500 MHz, CD_3OD)***: 175.2, 173.1, 172.3, 151.5, 149.5, 148.2, 146.3, 138.0, 132.2, 130.9, 122.4, 119.1, 112.8, 110.6, 109.1, 103.5, 72.4, 72.3, 71.4, 69.5, 44.1, 43.7, 35.4, 34.6, 33.8, 33.0, 24.6; ***LC-MS (ES-API)***: m/z = 915.3 $(M + H)^+$, ***IR***: 1703.1 cm^{-1}(C═O stretching); ***Mp***: 105–110 °C.

4.3. Computational analysis

4.3.1. Preparation of input files

The PDB files were gathered from the Protein Data Bank (PDB; accessible at https://www.rcsb.org/). The CRBN and target protein chains were purified to eliminate non-protein entities. The 5P9J structure (BTK1 co-crystallized with ibrutinib) was manually extracted from the PDB [21]. When the PROTAC was absent in the structure, other structures with the same domains and ligands were aligned, and the ligand coordinates were duplicated. Hydrogens were added to the ligands using UCSF Chimera, a software tool [34]. Side-chain repacking and minimization were performed after adding the protonated ligands to the structures. The ligand was replaced with its minimized equivalent to maintain the original coordinates and atom numbering. The SMILES representation of the linker was obtained from the PDB. If the structure was unavailable in the PDB, it was sourced from the research article where the structure was first described.

4.3.2. Protein-protein docking

The process of Protein-Protein docking was performed using HADDOCK [35]. The results include solutions to the protein-protein docking problem, which have been organized into clusters based on a 2 Å cut-off. A comprehensive evaluation was conducted on a maximum of 1000 docking solutions at a global scale for the subsequent phase. Specifically designed for docking, the procedure generates a maximum of 50 local docking outcomes for each global docking solution obtained using HADDOCK.

4.3.3. Generation of constrained PROTAC conformations for docking solutions

RDKit was used to generate up to 100 conformations of the PROTAC, adhering to the constraints imposed by the two ligands to ensure a proper fit within the local docking solution. This sampling process focuses exclusively on the linker conformation, keeping the conformation and position of the two ligands fixed. Due to the atom-distance-based limitations, the generated conformations may not initially align with the positions of ligands, necessitating an additional alignment step. After alignment, a threshold of 0.5 Å RMSD (Root Mean Square Deviation) was used to verify the congruence of each ligand with its corresponding X-ray conformation, ensuring the ligands' conformations accurately

match their natural states. The constraints in conformation generation in RDKit are crucial because generated conformations may not fully adhere to the specified constraints, primarily due to the reliance on atom distances during the process. The local docking position was discarded if no suitable conformation was achieved after 1000 trials.

4.3.4. Modeling PROTAC within the ternary complex

Rosetta's repack methodology was employed to select the most optimal PROTAC conformation from the set obtained in the preceding stage [21]. In this technique, the side chains of the residues are allowed to undergo rotamer switching. The constrained conformations generated using RDKit are provided as rotamers for the PROTAC, with the first conformation used as the initial rotamer. To align conformations based on a single atom (the nearby atom), the Rosetta Packer algorithm incorporates three virtual atoms with predetermined locations into the set of generated residue conformations. The central virtual atom has coordinates corresponding to the center of mass of the two ligands. Additionally, two other virtual atoms are positioned 1 Å from the central atom along the x and y axes. The central virtual atom is connected to two additional nearby atoms. This connection establishes a consistent 3D alignment, preventing the sampled conformations from being translated and avoiding any lever-arm effects. The repacking process is applied to the PROTAC molecule and any residual molecules within 10 Å. Following repacking, side-chain minimization was performed on the entire structure, except for the PROTAC molecule. Any models with a final score greater than or equal to 0 were eliminated from further consideration.

4.3.5. Clustering top scoring complexes

The DBSCAN clustering approach was used to group data [36]. Clusters were ranked based on the number of models they contained if clusters with a higher population corresponded to more optimal solutions. The DBSCAN algorithm can operate using either the coordinates of points in n dimensions or a distance matrix with precomputed distances between every pair of points. This study utilized Cα RMSD values of the moving chain, consistently defined as the target protein. Before performing the analysis, pairwise RMSD was calculated between the final solutions to create the distance matrix for the DBSCAN algorithm. The clustering process involved grouping the top 200 solutions, determined based on the interface score provided by Rosetta [37]. This score was calculated by subtracting the energy of the complex from the energy of the individual components after side-chain minimization. These top 200 solutions were selected from a pool of 1000 final solutions generated using Rosetta's repacking methodology. Clusters were ranked based on the number of structures they contained. For clusters of equal size, the ranking was determined by the average score of the final models. A native cluster was operationally defined as a cluster that includes at least one member with a Cα RMSD from the native conformation of less than 4 Å. The cluster reported in the study holds the highest rank among all native clusters.

4.4. Biology

4.4.1. Cell lines

All cell lines were obtained from ATCC (Middlesex, UK) and DSMZ (Braunschweig, Germany). Cells were maintained at 37 °C in a humidified incubator (5 % CO_2/atmospheric air) in the recommended growth medium, supplemented with 10 % fetal calf serum (Gibco), 1× Penicillin-Streptomycin solution (Diagnovum), 2 mM glutamine (Gibco), 1 mM Sodium bicarbonate (Gibco), 1 mM Sodium pyruvate (Gibco), and 20 mM HEPES (Gibco). All cell lines were routinely authenticated and checked for mycoplasma contamination fortnightly using established protocols in our laboratory [38,39].

4.4.2. Cytotoxicity assay

The cytotoxicity of all compounds in cell lines was assessed by a 3-(4,5-dimethylthiazol-2yl)-5-(3-carboxymethoxyphenyl)-2-(4-sulfophenyl)-2H-tetrazolium reduction assay after 72 h of treatment on a robotic high-throughput screening platform (HighResBio, Boston, MA, USA), using a standard protocol established in our laboratory [40]. IC_{50} calculation from dose-response curves of compounds was performed using Dotmatics (San Diego, CA, USA), as reported earlier [40]. The data was reported to chemists and archived via Portal MedChemBio (www.medchembio.imtm.cz).

4.4.3. Kinase assay

BTK and ITK kinase activity assays were performed using the BTK Kinase Enzyme System (Promega, Cat. #V2941) and ITK Kinase Assay Kit (BPS Biosciences, Inc., Cat. #78429) following the manufacturer's protocol with modifications. BTK and ITK enzymes were diluted to 5 ng/μL in 1× kinase reaction buffer provided in the respective kits. For BTK assays, the buffer was modified by adding 50 μM DTT and 2 mM $MnCl_2$, following manufacturer instructions. Serial dilutions of PROTAC **25** (0–10 μM) and ibrutinib (0–100 nM, MedChemExpress, Cat. #HY-10997) were prepared in 1× reaction buffer containing 10 % DMSO and dispensed at 1 μL per well in a 384-well white opaque plate (Corning, Part #4513). The final DMSO concentration was <0.5 % in all reaction wells. The kinase reaction was performed in a total volume of 5 μL, following the kit instructions. ADP production was detected using the ADP-Glo™ Kinase Assay (Promega, Cat. #V9101). Luminescence was measured using a Tecan Infinite 200 PRO plate reader (Tecan Group Ltd., Männedorf, Switzerland)) with an integration time of 1000 ms and a settle time of 200 ms. Enzyme activity (%) was calculated by normalizing luminescence values to DMSO control wells (100 % activity) and background wells (0 % activity). IC50 values were determined by a four-parameter logistic model (4PL) using GraphPad Prism (GraphPad Software, version 10; Boston, MA, USA).

4.4.4. Drug treatment and cell stimulation

RAMOS were plated in 6-well plates and treated with test compounds at 0–10 μM for 24 h to evaluate the BTK degrading activity of PROTACs. JURKAT cells were treated with PROTAC **25** at 0–20 μM concentrations for 24 h to examine its effect on protein levels of ITK. For bortezomib experiments, RAMOS cells were treated with 2× IC_{50} concentration of PROTAC **25** with or without 10 nM bortezomib (Sigma Aldrich) for 24 h. In LPS or IgM stimulation experiments, RAMOS cells were first treated with 2× IC_{50} concentration of PROTAC **25** for 24 h, followed by stimulation with 1 μg/mL LPS (Sigma Aldrich) or 10 μg/ F(ab')2-Goat anti-Human IgG, IgM (H + L) (Thermo Fisher, Cat. #16–5099-85) for 10 min. Drug-untreated cells were treated with DMSO at the same concentration in the highest tested drug concentration (the percentage of DMSO was always less than 0.5 %). Untreated and drug-treated cells were then collected and processed for Western blot analysis.

4.4.5. Western blotting

Cells were collected and washed twice with 1× PBS by centrifugation. The pelleted cells were suspended in RIPA buffer (Thermo Fisher Scientific, Massachusetts, USA; Cat. #89901) supplemented with protease inhibitors (Cat. #04693116001) and phosphatase inhibitors (Cat. #04906837001) obtained from Roche (Basel, Switzerland). The cells were lysed by sonication (25 % amplitude, 5 s off, 10 s on, for 1 min) using a Cup Horn Sonicator (Qsonica, LLC., Connecticut, USA) at 4 °C. The lysed cells were then centrifuged at 13000 ×*g* for 30 min at 4 °C using a benchtop centrifuge. The supernatant was collected in fresh, pre-chilled Eppendorf tubes and either analyzed immediately or stored at −80 °C for later use. The pelleted cell debris was discarded. The protein concentration in the supernatant was quantified using a BCA Protein Assay (Thermo Fisher Scientific, Massachusetts, USA, Cat. #23223 and Cat. #23224).

Proteins (30–40 μg) were separated by 10 % SDS-PAGE and then transferred to a nitrocellulose membrane (Cat. # 170–4270; Bio-Rad) using the Trans-Blot Turbo transfer system (Bio-Rad, California, USA).

The transferred membranes were blocked in 5 % BSA in 1 × Tris-Buffered Saline containing 0.1 % Tween® 20 detergent for 1 h at room temperature. Blocked membranes were then incubated with primary antibodies for 1 h at room temperature or overnight at 4 °C, followed by incubation with secondary antibodies for 1–2 h at room temperature in the dark. Images of blots were acquired using a Gel Doc XR + Gel Documentation System (Bio-Rad, California, USA) with appropriate filters for Alexa Fluor 488. Unless otherwise specified, all primary antibodies were purchased from Cell Signaling Technology, Inc. (Massachusetts, USA) and included: Total BTK (1:1000; Cat. #3533S), Total ITK (1:1000; Cat. # 2380S), Phospho (Tyr223) BTK (1:1000; Cat. # 5082S), M4G3LN Phospho (Tyr551, Tyr511) BTK/ITK (1 μg/mL, Cat. # 14–9015-82; Invitrogen, Massachusetts, USA), Total p38 MAPK (11,000; Cat. # 9212S), Phospho (Thr180/Tyr182) p38 MAPK (11,000; Cat. # 9211S), GAPDH (14 C10) (14,000; Cat # 2118S), and α-Tubulin (12,000; Cat. # T51687, Sigma Aldrich). All secondary antibodies were purchased from Invitrogen (Massachusetts, USA) and included anti-mouse IgG Alexa Fluor 488 (12,000; Cat. #A11034) and anti-rabbit IgG Alexa Fluor 488 (12,000; Cat. #A21202).

4.4.6. Blot analysis and statistical analysis

Blots were analyzed using ImageJ software (v1.54). Total and phosphorylated protein band intensities were normalized to their respective loading controls (GAPDH or α-Tubulin), with phosphorylated protein levels expressed relative to their respective total protein levels.

DC_{50} and Dmax values were determined from dose-response curves generated using quantitative Western blot data, as elsewhere [41]. Briefly, the percentage of protein remaining was calculated relative to the DMSO-treated control (set to 100 %), and degradation (%) was then determined using the formula: [1 – (Normalized Band Intensity of Treated Sample/ Normalized Band Intensity of DMSO Control)] × 100. Degradation values were fitted to a 4PL model in GraphPad Prism to determine DC_{50}. Dmax was calculated from the bottom plateau of the fitted curve, using Dmax = 100 – Bottom, where Bottom represents the lowest plateau of the fitted degradation curve. The analysis was conducted using the method described elsewhere[41].

Statistical analyses were performed using GraphPad Prism software, and differences were considered significant at $P < 0.05$.

CRediT authorship contribution statement

Naveen Kumar Rampeesa: Writing – original draft, Methodology, Investigation. **Rambabu Gundla:** Writing – review & editing, Supervision, Project administration, Funding acquisition, Conceptualization. **Gopal Mudasani:** Investigation, Data curation. **Sudhakar Tangallapalli:** Methodology, Investigation. **Sreenivasa Reddy Anugu:** Resources. **Soňa Gurská:** Methodology, Investigation. **Juan Bautista De Sanctis:** Methodology, Investigation. **Petr Džubák:** Resources, Funding acquisition. **Marián Hajdúch:** Writing – review & editing, Resources, Funding acquisition. **Viswanath Das:** Writing – review & editing, Supervision, Project administration, Investigation, Funding acquisition, Conceptualization.

Declaration of competing interest

The authors declare the following financial interests/personal relationships which may be considered as potential competing interests: Gopal Muddasani and Naveen Kumar Rampeesa report equipment, drugs, or supplies were provided by Aragen life sciences private limited. Gopal Muddasani and Naveen Kumar Rampeesa report equipment, drugs, or supplies were provided by NATCO research center, Hyderabad, Telangana. Gopal Muddasani and Naveen Kumar Rampeesa report a relationship with Aragen life sciences private limited that includes: Employment. Gopal Muddasani has patent #Azaspirooxindolinone derivatives and the use of same in cancer therapy (Indian patent application no. 202441059533 A) pending to GITAM deemed to be university. Naveen Kumar Rampeesa has patent #Azaspirooxindolinone derivatives and the use of same in cancer therapy (Indian patent application no. 202441059533 A) pending to GITAM deemed to be university. Sreenivasa Anugu has patent #Azaspirooxindolinone derivatives and the use of same in cancer therapy (Indian patent application no. 202441059533 A) pending to GITAM deemed to be university. Viswanath Das has patent #Azaspirooxindolinone derivatives and the use of same in cancer therapy (Indian patent application no. 202441059533 A) pending to GITAM deemed to be university. Rambabu Gundla has patent #Azaspirooxindolinone derivatives and the use of same in cancer therapy (Indian patent application no. 202441059533 A) pending to GITAM deemed to be university. Both Gopal Muddasani and Naveen Kumar Rampeesa are empolyees of Aragen Lifesciences Pvt. ltd., and doctoral students at GITAM deemed to be university. Naveen Kumar Rampeesa, Rambabu Gundla, Gopal Mudasani, Sreenivasa Anugu, and Viswanath Das are listed as inventors on a published patent application titled "Azaspirooxindolinone based PROTAC compounds to target ITK and BTK kinases", Indian Patent Application No. 202441059537 A. If there are other authors, they declare that they have no known competing financial interests or personal relationships that could have appeared to influence the work reported in this paper.

Acknowledgements

Dr. Rambabu Gundla acknowledges DBT-BIRAC (BT/AIR01566/PACE-27/22) for financial assistance and GITAM University, Hyderabad, India, for the facility. RN and RG thank Aragen Lifesciences Pvt. Ltd., Hyderabad, India, for providing computational resources for synthesizing and characterizing all the compounds by NMR, LC-MS, and FT-IR. All biological part of the study was supported in parts by the infrastructural projects (CZ-OPENSCREEN – LM2023052; EATRIS-CZ – LM2023053), the Czech biobank network (BBMRI - LM2023033), the projects National Institute for Cancer Research (Program EXCELES, ID Project No. LX22NPO5102) and National Institute for Neurological Research (Program EXCELES, ID Project No. LX22NPO5107) - Funded by the European Union - Next Generation EU from the Ministry of Education, Youth and Sports of the Czech Republic (MEYS), project TN02000109 (Personalized Medicine: From Translational Research into Biomedical Applications is co-financed with the state support of the Technology Agency of the Czech Republic as part of the National Centers of Competence Program), and project SALVAGE (registration number: CZ.02.01.01/00/22_008/0004644, supported by OP JAK, with co-financing from the EU and the State Budget).

Appendix A. Supplementary data

Supporting Material contains the characterization of all compounds (^{1}H NMR, ^{13}C NMR, FT-IR spectra, and LC/MS), representative IC_{50} curves, supplementary cytotoxicity method and table, and images of full western blots. Supplementary data to this article can be found online at [https://doi.org/10.1016/j.bioorg.2025.108316].

Data availability

All data supporting the findings of this study are available in the manuscript or supplementary material.

References

[1] L.J. Berg, L.D. Finkelstein, J.A. Lucas, P.L. Schwartzberg, Tec family kinases in T lymphocyte development and function, Annu. Rev. Immunol. 23 (2004) 549–600, https://doi.org/10.1146/annurev.immunol.22.012703.104743.

[2] J.A. Readinger, K.L. Mueller, A.M. Venegas, R. Horai, P.L. Schwartzberg, Tec kinases regulate T-lymphocyte development and function: new insights into the roles of Itk and Rlk/Txk, Immunol. Rev. 228 (2009) 93–114, https://doi.org/10.1111/j.1600-065X.2008.00757.x.

[3] B. Ye, C. Zhou, H. Guo, M. Zheng, Effects of BTK signalling in pathogenic microorganism infections, J. Cell. Mol. Med. 23 (2019) 6522–6529, https://doi.org/10.1111/jcmm.14548.

[4] C. McDonald, C. Xanthopoulos, E. Kostareli, The role of Bruton's tyrosine kinase in the immune system and disease, Immunology 164 (2021) 722–736, https://doi.org/10.1111/imm.13416.

[5] S. Volmering, H. Block, M. Boras, C.A. Lowell, A. Zarbock, The neutrophil Btk signalosome regulates integrin activation during sterile inflammation, Immunity 44 (2016) 73–87, https://doi.org/10.1016/j.immuni.2015.11.011.

[6] K. Maddocks, Update on mantle cell lymphoma, Blood 132 (2018) 1647–1656, https://doi.org/10.1182/blood-2018-03-791392.

[7] E. Dolgin, BTK blockers make headway in multiple sclerosis, Nat. Biotechnol. 39 (2021) 3–5, https://doi.org/10.1038/s41587-020-00790-7.

[8] A.D. Buhimschi, H.A. Armstrong, M. Toure, S. Jaime-Figueroa, T.L. Chen, A. M. Lehman, J.A. Woyach, A.J. Johnson, J.C. Byrd, C.M. Crews, Targeting the C481S Ibrutinib-resistance mutation in Bruton's tyrosine kinase using PROTAC-mediated degradation, Biochemistry 57 (2018) 3564–3575, https://doi.org/10.1021/acs.biochem.8b00391.

[9] Y.-Q. Li, W.G. Lannigan, S. Davoodi, F. Daryaee, A. Corrionero, P. Alfonso, J. A. Rodriguez-Santamaria, N. Wang, J.D. Haley, P.J. Tonge, Discovery of novel Bruton's tyrosine kinase PROTACs with enhanced selectivity and cellular efficacy, J. Med. Chem. 66 (2023) 7454–7474, https://doi.org/10.1021/acs.jmedchem.3c00176.

[10] J.R. Brown, Ibrutinib (PCI-32765), the first BTK (Bruton's tyrosine kinase) inhibitor in clinical trials, Curr. Hematol. Malig. Rep. 8 (2013) 1–6, https://doi.org/10.1007/s11899-012-0147-9.

[11] R. Gabizon, A. Shraga, P. Gehrtz, E. Livnah, Y. Shorer, N. Gurwicz, L. Avram, T. Unger, H. Aharoni, S. Albeck, A. Brandis, Z. Shulman, B.-Z. Katz, Y. Herishanu, N. London, Efficient targeted degradation via reversible and irreversible covalent PROTACs, J. Am. Chem. Soc. 142 (2020) 11734–11742, https://doi.org/10.1021/jacs.9b13907.

[12] G. Xue, J. Chen, L. Liu, D. Zhou, Y. Zuo, T. Fu, Z. Pan, Protein degradation through covalent inhibitor-based PROTACs, Chem. Commun. 56 (2020) 1521–1524, https://doi.org/10.1039/C9CC08238G.

[13] Y. Sun, X. Zhao, N. Ding, H. Gao, Y. Wu, Y. Yang, M. Zhao, J. Hwang, Y. Song, W. Liu, Y. Rao, PROTAC-induced BTK degradation as a novel therapy for mutated BTK C481S induced ibrutinib-resistant B-cell malignancies, Cell Res. 28 (2018) 779–781, https://doi.org/10.1038/s41422-018-0055-1.

[14] D.W. Robbins, M.A. Noviski, Y.S. Tan, Z.A. Konst, A. Kelly, P. Auger, N. Brathaban, R. Cass, M.L. Chan, G. Cherala, M.C. Clifton, S. Gajewski, T.G. Ingallinera, D. Karr, D. Kato, J. Ma, J. McKinnell, J. McIntosh, J. Mihalic, B. Murphy, J.R. Panga, G. Peng, J. Powers, L. Perez, R. Rountree, A. Tenn-McClellan, A.T. Sands, D. R. Weiss, J. Wu, J. Ye, C. Guiducci, G. Hansen, F. Cohen, Discovery and preclinical pharmacology of NX-2127, an orally bioavailable degrader of Bruton's tyrosine kinase with immunomodulatory activity for the treatment of patients with B cell malignancies, J. Med. Chem. 67 (2024) 2321–2336, https://doi.org/10.1021/acs.jmedchem.3c01007.

[15] N. Sahu, A. August, ITK inhibitors in inflammation and immune-mediated disorders, Curr. Top. Med. Chem. 9 (2009) 690–703, https://doi.org/10.2174/156802609789044443.

[16] G. Mudasani, K. Paidikondala, S. Gurská, S.J. Maddirala, P. Džubák, V. Das, R. Gundla, C-5 aryl substituted Azaspirooxindolinones derivatives: synthesis and biological evaluation as potential inhibitors of Tec family kinases, Eur. J. Org. Chem. 2021 (2021) 4630–4640, https://doi.org/10.1002/ejoc.202100699.

[17] W.-H. Guo, X. Qi, X. Yu, Y. Liu, C.-I. Chung, F. Bai, X. Lin, D. Lu, L. Wang, J. Chen, L.H. Su, K.J. Nomie, F. Li, M.C. Wang, X. Shu, J.N. Onuchic, J.A. Woyach, M. L. Wang, J. Wang, Enhancing intracellular accumulation and target engagement of PROTACs with reversible covalent chemistry, Nat. Commun. 11 (2020) 4268, https://doi.org/10.1038/s41467-020-17997-6.

[18] J. Madan, V.K. Ahuja, K. Dua, S. Samajdar, M. Ramchandra, S. Giri, PROTACs: current trends in protein degradation by proteolysis-targeting chimeras, BioDrugs 36 (2022) 609–623, https://doi.org/10.1007/s40259-022-00551-9.

[19] S. Kregel, C. Wang, X. Han, L. Xiao, E. Fernandez-Salas, P. Bawa, B.L. McCollum, K. Wilder-Romans, I.J. Apel, X. Cao, C. Speers, S. Wang, A.M. Chinnaiyan, Androgen receptor degraders overcome common resistance mechanisms developed during prostate cancer treatment, Neoplasia 22 (2020) 111–119, https://doi.org/10.1016/j.neo.2019.12.003.

[20] Z. Liu, M. Hu, Y. Yang, C. Du, H. Zhou, C. Liu, Y. Chen, L. Fan, H. Ma, Y. Gong, Y. Xie, An overview of PROTACs: a promising drug discovery paradigm, Mol. Biomed. 3 (2022) 46, https://doi.org/10.1186/s43556-022-00112-0.

[21] A.T. Bender, A. Gardberg, A. Pereira, T. Johnson, Y. Wu, R. Grenningloh, J. Head, F. Morandi, P. Haselmayer, L. Liu-Bujalski, Ability of Bruton's tyrosine kinase inhibitors to sequester Y551 and prevent phosphorylation determines potency for inhibition of fc receptor but not B-cell receptor signaling, Mol. Pharmacol. 91 (2017) 208, https://doi.org/10.1124/mol.116.107037.

[22] C.P. Koraboina, V.C. Maddipati, N. Annadurai, S. Gurská, P. Džubák, M. Hajdúch, V. Das, R. Gundla, Synthesis and Biological Evaluation of Oxindole Sulfonamide Derivatives as Bruton's Tyrosine Kinase Inhibitors**, ChemMedChem n/a (2023) e202300511, https://doi.org/10.1002/cmdc.202300511.

[23] R.D. Medh, M.S. Webb, A.L. Miller, B.H. Johnson, Y. Fofanov, T. Li, T.G. Wood, B. A. Luxon, E.B. Thompson, Gene expression profile of human lymphoid CEM cells sensitive and resistant to glucocorticoid-evoked apoptosis, Genomics 81 (2003) 543–555, https://doi.org/10.1016/S0888-7543(03)00045-4.

[24] E. Pastwa, R.I. Somiari, M. Malinowski, S.B. Somiari, T.A. Winters, In vitro non-homologous DNA end joining assays—the 20th anniversary, Int. J. Biochem. Cell Biol. 41 (2009) 1254–1260, https://doi.org/10.1016/j.biocel.2008.11.007.

[25] S. Nisitani, R.M. Kato, D.J. Rawlings, O.N. Witte, M.I. Wahl, In situ detection of activated Bruton's tyrosine kinase in the Ig signaling complex by phosphopeptide-specific monoclonal antibodies, Proc. Natl. Acad. Sci. 96 (1999) 2221–2226, https://doi.org/10.1073/pnas.96.5.2221.

[26] D. Akasaka, S. Iguchi, R. Kaneko, Y. Yoshiga, D. Kajiwara, Y. Nakachi, N. Noma, K. Tanaka, A. Shimizu, F. Hosoi, Novel Bruton's tyrosine kinase inhibitor TAS5315 suppresses the progression of inflammation and joint destruction in rodent collagen-induced arthritis, PLoS One 18 (2023) e0282117, https://doi.org/10.1371/journal.pone.0282117.

[27] L. Ping, N. Ding, Y. Shi, L. Feng, J. Li, Y. Liu, Y. Lin, C. Shi, X. Wang, Z. Pan, Y. Song, J. Zhu, The Bruton's tyrosine kinase inhibitor ibrutinib exerts immunomodulatory effects through regulation of tumor-infiltrating macrophages, Oncotarget 8 (24) (2017). https://www.oncotarget.com/article/16836/text/ (accessed January 1, 2017).

[28] T. Kurosaki, M. Kurosaki, Transphosphorylation of Bruton's tyrosine kinase on tyrosine 551 is critical for B cell antigen receptor function *, J. Biol. Chem. 272 (1997) 15595–15598, https://doi.org/10.1074/jbc.272.25.15595.

[29] G. Mudasani, K. Paidikondala, R. Gundla, S. Joseph Maddirala, V. Das, Synthesis and biological evaluation of 5′-Arylspiro[piperidine-4,3′-pyrrolo-[2,3-b]pyridin] analogues, ChemistrySelect 6 (2021) 3378–3381, https://doi.org/10.1002/slct.202004719.

[30] J. Qi, S. Armstrong, L. Wu, Compounds, compositions, and methods for protein degradation, WO2020264172A1. https://patents.google.com/patent/WO2020264172A1/en?oq=+WO2020%2f264172, 2020 (accessed June 7, 2024).

[31] H. Wang, C. Huo, Y. Guo, R. Qi, Z. Wang, Degradation of bruton's tyrosine kinase (btk) by conjugation of btk inidbitors with e3 ligase ligand and methods of use, WO2021018018A1. https://patents.google.com/patent/WO2021018018A1/en?oq=WO2021018018, 2021.

[32] X. Zhang, D. Thummuri, X. Liu, W. Hu, P. Zhang, S. Khan, Y. Yuan, D. Zhou, G. Zheng, Discovery of PROTAC BCL-XL degraders as potent anticancer agents with low on-target platelet toxicity, Eur. J. Med. Chem. 192 (2020) 112186, https://doi.org/10.1016/j.ejmech.2020.112186.

[33] R. Lun, Z. Fengying, S. Xiuyun, Z. Gang, Y. Zimo, S. Yonghui, L. Xuemei, Preparation of isoindoline derivatives as degradation agent targeting both BTK and GSPT1 proteins and its application, CN115304606A. https://patents.google.com/patent/CN115304606A/zh?oq=CN115304606, 2022 (accessed June 7, 2024).

[34] E.F. Pettersen, T.D. Goddard, C.C. Huang, G.S. Couch, D.M. Greenblatt, E.C. Meng, T.E. Ferrin, UCSF chimera—a visualization system for exploratory research and analysis, J. Comput. Chem. 25 (2004) 1605–1612, https://doi.org/10.1002/jcc.20084.

[35] G.C.P. van Zundert, J.P.G.L.M. Rodrigues, M. Trellet, C. Schmitz, P.L. Kastritis, E. Karaca, A.S.J. Melquiond, M. van Dijk, S.J. de Vries, A.M.J.J. Bonvin, The HADDOCK2.2 web server: user-friendly integrative modeling of biomolecular complexes, J. Mol. Biol. 428 (2016) 720–725, https://doi.org/10.1016/j.jmb.2015.09.014.

[36] M. Ester, H.-P. Kriegel, J. Sander, X. Xu, A Density-Based Algorithm for Discovering Clusters in Large Spatial Databases with Noise, 1996, pp. 226–231.

[37] S.J. Fleishman, A. Leaver-Fay, J.E. Corn, E.-M. Strauch, S.D. Khare, N. Koga, J. Ashworth, P. Murphy, F. Richter, G. Lemmon, J. Meiler, D. Baker, RosettaScripts: a scripting language Interface to the Rosetta macromolecular modeling suite, PLoS One 6 (2011) e20161, https://doi.org/10.1371/journal.pone.0020161.

[38] R. Buriánová, J. Kotulová, Detection of mycoplasma contamination in cell lines by PCR (Chapter 5), in: J. Drábek, V. Das, P. Dzubak, Josef Strovnal, J. Bouchal, M. Hajduch, K. Koberna, A. Ligasová, M. Mistrik, J. De Sanctis (Eds.), Laboratory Techniques in Cellular and Molecular Medicine, 1st ed., Palacký University Olomouc, Olomouc, 2022, pp. 37–42, https://doi.org/10.5507/lf.22.24460499.

[39] J. Stránská, STR profiling for cell line authentication (Chapter 4), in: J. Drábek, V. Das, P. Dzubak, Josef Strovnal, J. Bouchal, M. Hajduch, K. Koberna, A. Ligasová, M. Mistrik, J. De Sanctis (Eds.), Laboratory Techniques in Cellular and Molecular Medicine, 1st ed., Palacký University Olomouc, Olomouc, Olomouc, 2022, pp. 29–36, https://doi.org/10.5507/lf.22.24460499.

[40] S. Gurská, Analysis of cytotoxicity by tetrazolium salt reduction test (Chapter 10), in: J. Drábek, V. Das, P. Dzubak, Josef Strovnal, J. Bouchal, M. Hajduch, K. Koberna, A. Ligasová, M. Mistrik, J. De Sanctis (Eds.), Laboratory Techniques in Cellular and Molecular Medicine, 1st ed., Palacký University Olomouc, Olomouc, 2022, pp. 67–72, https://doi.org/10.5507/lf.22.24460499.

[41] X. Ji, L. Miao, Y. Wu, T. Zhao, Y. Si, X. Tan, Q. Zhou, R. Zuo, J. Pei, J. Wu, C. Ma, Z. Ma, D. Xu, A rapid and accurate method for evaluating the degradation of pan-Akt in cells by PROTACs using NanoLuc luciferase, Biology Methods Protocols 9 (2024) bpae014, https://doi.org/10.1093/biomethods/bpae014.